Nano-Segregation and Structuring in the Bulk and at the Surface of Ionic-Liquid Mixtures

Nano-Segregation and Structuring in the Bulk and at the Surface of Ionic-Liquid Mixtures

Duncan W. Bruce[1],* Christopher P. Cabry[1], José N. Canongia Lopes[4,5],* Matthew L. Costen[2],* Lucía D'Andrea[1], Isabelle Grillo[7], Brooks C. Marshall[3], Kenneth G. McKendrick[2],* Timothy K. Minton[3],* Simon M. Purcell[2], Sarah Rogers[6], John M. Slattery[1],* Karina Shimizu[4,5], Eric Smoll[3], María A. Tesa-Serrate[2]

[1]*Department of Chemistry, University of York, Heslington, York YO10 5DD, UK*

[2]*Institute of Chemical Sciences, Heriot-Watt University, Edinburgh EH14 4AS, UK*

[3]*Department of Chemistry and Biochemistry, Montana State University, Montana 59717, USA*

[4]*Centro de Química Estrutural, IST, Universidade de Lisboa, 1049-001 Lisboa, Portugal*

[5]*ITQB, Universidade Nova de Lisboa, Avenida República, 2780-157 Oeiras, Portugal*

[6]*ISIS, Science & Technology Facilities Council, Rutherford Appleton Laboratory, Chilton, UK*

[7]*ILL, 71 Avenue des Martyrs, CS 20156-38042, Grenoble Cedex 9, France*

Abstract

Ionic-liquid (IL) mixtures hold great promise, as they allow liquids with a wide range of properties to be formed by mixing two common components, rather than by synthesizing a large array of pure ILs with different chemical structures. In addition, these mixtures can exhibit a range of properties and structural organization that depend on their composition, which opens up new possibilities for the composition-dependent control of IL properties for particular applications. However, the fundamental properties, structure and dynamics of IL mixtures are currently poorly understood, which limits their more widespread application. This paper presents the first comprehensive investigation into the bulk and surface properties of IL mixtures formed from two commonly encountered ILs: 1-ethyl-3-methylimidazolium and 1-dodecyl-3-methylimidazolium bis(trifluoromethylsulfonyl)imide

([C_2mim][Tf_2N] and [C_{12}mim][Tf_2N]). Physical property measurements (viscosity, conductivity and density) find that these IL mixtures are not well described by simple mixing laws, suggesting that their structure and dynamics are strongly composition-dependent. Small-angle X-ray and neutron scattering (SAXS and SANS) measurements, alongside molecular dynamics (MD) simulations, show that at low mole fractions of [C_{12}mim][Tf_2N], the bulk of the IL is composed of small aggregates of [C_{12}mim]$^+$ ions in a [C_2mim][Tf_2N] matrix, which is driven by nano-segregation of the long alkyl chains and the polar parts of the IL. As the proportion of [C_{12}mim][Tf_2N] in the mixtures increases, the size and number of aggregates increases until the C12 alkyl chains percolate through the system and a bicontinuous network of polar and non-polar domains is formed. Reactive atom scattering-laser-induced fluorescence (RAS-LIF) experiments, also supported by MD simulations, have been used to probe the surface structure of these mixtures. It is found that the vacuum-IL interface is enriched significantly in C12 alkyl chains, even in mixtures low in the long-chain component. These data show, contrary to previous suggestions, that the [C_{12}mim]$^+$ ion is surface active in this binary IL mixture. However, the surface does not become saturated in C12 chains as its proportion in the mixtures increases and remains unsaturated in pure [C_{12}mim][Tf_2N].

Introduction

Ionic liquids (ILs) are molten salts that are liquid at relatively low temperatures. They are often defined as salts with melting temperatures below 100 °C, but a great many are liquid at room temperature and below. There has been much interest in ILs in recent years and their unusual combination of properties, such as very low vapor pressures, wide electrochemical windows, good thermal stabilities, and ability to dissolve a wide range of solutes, has led to their use in a range of areas. These include as reaction media for sustainable chemistry and catalysis;[1-10] in the electrochemical deposition of metals and semiconductors;[1, 11-16] nanoscience;[17-23] biomass processing;[24] carbon capture and storage (CCS);[25-26] analytical chemistry[27-32] and many more.

One of the advantages of ILs is that their properties can be altered substantially by changing the anion, cation or both. This offers significant potential to tune the properties of an IL for a particular application; for this reason, ILs are often described as 'designer solvents'. However, the

2

downside of this flexibility is that there are a huge number of potential combinations of ions that will form ILs and it would be impossible to synthesize and test all of these for every application. Recent studies have shown that it is possible to generate a library of liquids with a range of properties by simply mixing two or more ILs.[33-34] As such, IL mixtures offer the attractive prospect of being able to access a range of properties from a relatively small number of common ILs by mixing, rather than having to synthesize and store large numbers of different ILs. However, while significant progress has been made in recent years in our understanding of pure ILs,[35-36] comparatively little is known about the fundamental properties of IL mixtures and how these relate to their composition.

The structure and dynamics of ILs, both in the bulk and at the gas-liquid interface, are critical to many of their applications. In the bulk, the amphiphilic nature of many IL ions results in nano-segregation of the liquid into polar and non-polar domains,[37] leading to the development of nanostructure that has been studied using a range of experimental and computational approaches.[35] Considerably less is known about the effects of mixing ILs on their nanostructure, or indeed their fundamental physical properties compared to pure ILs. Some reports of physicochemical investigations of IL mixtures have found that they exhibit properties that are quite well described by simple mixing laws,[38-53] although this is somewhat surprising given that the chemical structures of some of the ions involved are significantly different. However, non-ideal behavior has also been observed in other studies (*e.g.* of conductivity,[40-41, 54-56] density,[46, 50, 57-59] viscosity[48, 52, 60-61] and phase behavior[62]) and, interestingly, some IL mixtures that display ideal mixing behavior in some of their physical properties exhibit significantly non-ideal behavior in others. This has led to the suggestion that IL mixtures are best considered as 'double salt ionic liquids' (DSILs)[34] whose properties are defined by their ultimate ionic composition, rather than by the properties of the pure ILs from which they are derived.

In most cases the origins of non-ideal behavior in IL mixtures are not well understood, but factors such as size differences between the cations and/or the different hydrogen-bonding abilities of ions in a mixture have been proposed as important.[34, 48] As is so often the case with ILs, general explanations for these phenomena that apply to all of the diverse range of ILs that are known are unlikely to be found. Instead, detailed experimental and theoretical investigation of a range of

different types of IL mixtures is important to understand their behavior.[42, 63-69] One area that has not

received significant attention, but is likely to play a key role in dictating the properties of IL mixtures,

is the nanostructure that results from aggregation of one IL in another. A small number of studies

have investigated the self-organization of ionic amphiphiles (*e.g.* long-chain imidazolium, pyridinium

and piperidinium halide or $[BF_4]^-$ salts) in both protic $([EtNH_3][NO_3])$[70-76] and aprotic $([C_4mim][Tf_2N]$

and $[C_nmim][FeCl_4]$ ($n = 2$ and 4))[77-79] ILs. It is also well known that ILs can be used as solvents for

the self-organization of non-ionic surfactants.[80-81] What is currently unclear is the extent to which self-

organization plays a role in the observed properties of IL mixtures containing ions that are more

similar in their chemical structure. To the best of our knowledge there have been no reports of self-

organization (*i.e.* aggregation/micelle formation) in binary IL mixtures (mixtures containing a

common anion and two different cations or *vice versa*).

　　　　The structures of IL surfaces have also been studied in some detail and are of particular

interest in applications where the gas–liquid interface is important *e.g.* CCS, multi-phase catalysis and

gas separation. A range of approaches have been used to study IL surfaces and some general features

and design rules are beginning to emerge, although there is still much to learn in this area.[36, 82-86] IL

surface structure is influenced by variations of both the anion and cation and, within a series of ILs,

increasing the alkyl chain length on the cation leads to a surface that is less polar and more saturated

with alkyl chains.[87] Moving from large anions (*e.g.* $[Tf_2N]^-$) to smaller anions (*e.g.* $[BF_4]^-$) for a given

chain length increases the density of alkyl chains at the surface, due to more efficient packing of the

ions.[83] However, there have been relatively few investigations into the surface structure of IL

mixtures.[67, 84, 88-89] Information of the surface structure can be obtained from indirect classical

measurements such as surface tension measurements, which we do not consider further here. More

direct experimental techniques used include angle-resolved X-ray photoelectron spectroscopy

(ARXPS),[90] Rutherford backscattering spectroscopy (RBS),[86, 91] low-energy ion scattering (LEIS)[82]

and time-of-flight secondary ion mass spectrometry (ToF-SIMs),[86, 92] and the technique which we

have pioneered and use here, reactive-atom scattering with laser-induced fluorescence detection

(RAS-LIF).[83, 93-94] They have also been investigated by MD simulations.[95-96] There are large

discrepancies in the degree of surface enrichment reported, ranging from stoichiometric surface

4

compositions (detected by ARXPS)[90] to the complete absence of some constituting ions at the surface (reported in an LEIS study).[82] It should be noted that these studies were concerned with different IL combinations, which might have distinct mixing behaviors. However, the same IL mixture investigated using two techniques (RBS and ToF-SIMs) showed different surface compositions.[86]

$(n = 2)$ [C$_2$mim]$^+$
$(n = 12)$ [C$_{12}$mim]$^+$

[TF$_2$N]$^-$
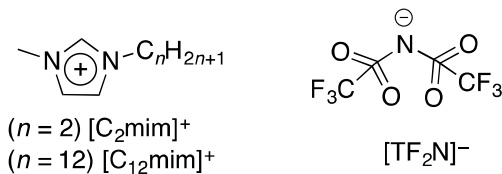
Figure 1: The chemical structures of the IL ions used here.

This work provides a detailed picture of the physical properties and structure (in the bulk and at the gas-liquid interface) of binary IL mixtures that display properties that deviate significantly from ideal mixing behavior. The mixtures of interest are formed from two imidazolium ILs: [C$_2$mim][Tf$_2$N] and [C$_{12}$mim][Tf$_2$N] (figure 1) in various proportions (these mixtures will be denoted [C$_2$mim]$_{1-x}$[C$_{12}$mim]$_x$[Tf$_2$N], where $x = 0$ to 1).[33, 53] By mixing an IL with no nanostructure, [C$_2$mim][Tf$_2$N] (figure 2, left), with one containing the amphiphilic cation, [C$_{12}$mim][Tf$_2$N] (figure 2, right), which is known to form a nano-segregated structure in the bulk and display significant surface ordering, interesting bulk and surface phenomena are observed.[87, 93-94] This is the first time that many of these features have been reported, and that a unified discussion of both bulk and surface properties has been presented for binary IL mixtures.
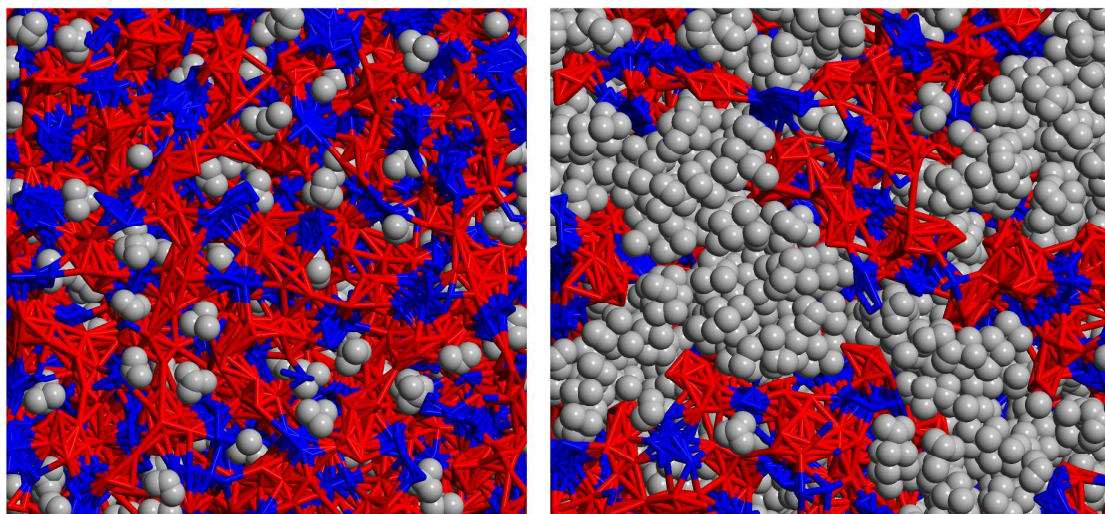
Figure 2: MD simulation snapshots illustrating the bulk-phase structure of $[C_2mim][Tf_2N]$ (left) and $[C_{12}mim][Tf_2N]$ (right).[97] Atoms associated with the $[Tf_2N]^-$ ion are colored red. For $[C_2mim]^+$ and $[C_{12}mim]^+$ ions, the methyl substituent, imidazolium ring and the first methylene group of the alkyl substituent are shown in blue. All other atoms of the $[C_{12}mim]^+$ and $[C_2mim]^+$ cation alkyl substituents are shown in grey. Nano-segregation between the polar network (red/blue mesh) and non-polar domains (grey and green beads) can be seen in $[C_{12}mim][Tf_2N]$, but no nano-segregation is seen in $[C_2mim][Tf_2N]$.

Results

The bulk properties of $[C_2mim]_{1-x}[C_{12}mim]_x[Tf_2N]$ mixtures ($x = 0$ to 1) were investigated by measuring physical properties (viscosity, conductivity and density), as well as with SANS and SAXS experiments, and MD simulations. The structure of the vacuum-liquid interface was investigated using reactive-atom scattering probed *via* laser-induced-fluorescence (RAS-LIF) and MD simulations. As such, this is a most extensive characterization of bulk and surface properties of these mixtures.

Physical property measurements

The viscosity and conductivity of ILs are known to be quite sensitive to the nature of both the anion and cation. However, in previous work on IL mixtures, composition-dependent viscosities and

6

conductivities have often been found to be quite well described by simple mixing laws. In particular, the Arrhenius or Grunberg-Nissan mixing law:[98-100]

$$\log \eta = x\log \eta_1 + (1-x)\log \eta_2 \quad (1)$$

(where x is the mole fraction of one component of a binary mixture and η, η_1 and η_2 are the viscosity of the mixture, component 1 and component 2, respectively) or the Katti and Chaudhri mixing law:[101]

$$\log \eta V_m = x\log \eta_1 V_{m,1} + (1-x)\log \eta_2 V_{m,2} + \frac{\Delta G^E}{RT} \quad (2)$$

(where V_m, $V_{m,1}$ and $V_{m,2}$ are the molar volumes of the mixture and the two components, respectively, and ΔG^E is the excess molar Gibbs energy of activation for flow).

Temperature-dependent viscosities and ionic conductivities were measured for at least twelve compositions of $[C_2mim]_{1-x}[C_{12}mim]_x[Tf_2N]$ from 293 to 333 K (see ESI for details). The temperature dependence of both the viscosity and conductivity data fitted well to the Vogel-Fulcher-Tammann (VFT) equation for glass-forming systems (full experimental data and fitting is given in the ESI) and all ILs behaved as Newtonian fluids under the sheer-rate range used. The viscosities of mixtures in the $[C_2mim]_{1-x}[C_{12}mim]_x[Tf_2N]$ system are poorly described by a linear mixing law:

$$\eta = x\eta_1 + (1-x)\eta_2 \quad (3)$$

as expected for ILs (see ESI for details). However, large deviations from ideal mixing behavior are also seen when using the Grunberg-Nissan mixing law (figure 3). Attempted fitting of the data to the Katti and Chaudhri mixing law showed similar behavior, as the molar volumes of mixtures in this system show only small deviations from ideal mixing behavior with changing composition (*vide infra*).

Figure 3 (black squares) shows that according to the Grunberg-Nissan mixing law, at low $[C_{12}mim][Tf_2N]$ loadings (up to 16 mol%) the viscosity of the mixtures behaves in essentially an ideal way (within the error of the experiment), but from the 24 mol% point onwards there is a significant deviation, which appears greatest at around 50 mol% $[C_{12}mim][Tf_2N]$. In this region, the IL mixtures show a positive deviation and are more viscous than would be expected based on the Grunberg-Nissan law.
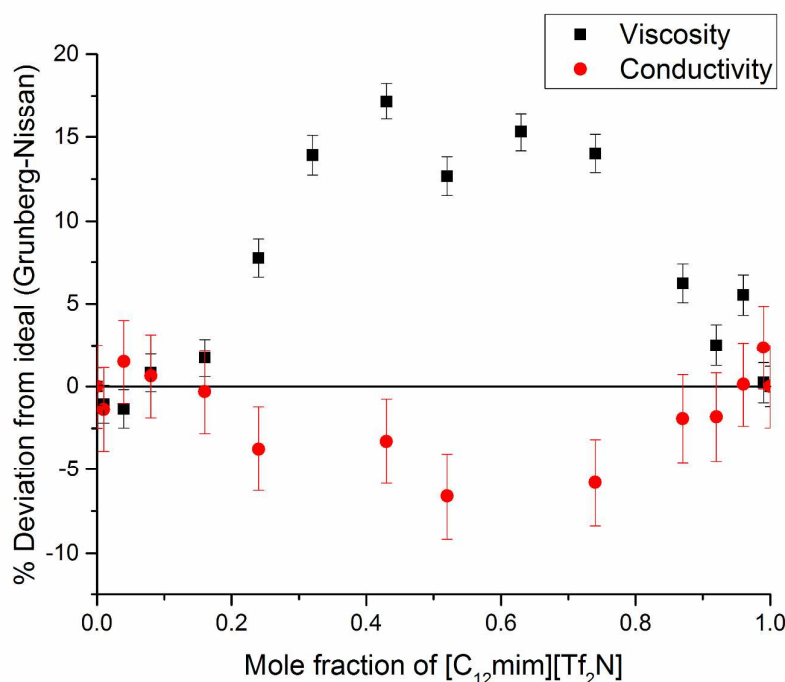
Figure 3: Percentage deviation of viscosity and conductivity (at 293 K) from the Grunberg-Nissan

mixing law for $[C_2mim]_{1-x}[C_{12}mim]_x[Tf_2N]$ mixtures as a function of composition.

Conductivity measurements on the $[C_2mim]_{1-x}[C_{12}mim]_x[Tf_2N]$ mixtures give a similar picture

(figure 3, red circles), although the conductivity data deviate less significantly from the Grunberg-

Nissan mixing law compared to the viscosity data. Again, there is a significant (within experimental

error) difference between the observed and predicted conductivity from 24 mol% $[C_{12}mim][Tf_2N]$

onwards, being greatest at around 50 mol%. In the region where there is a significant difference

between the observed and predicted conductivities, the mixtures have lower conductivities than

expected from Grunberg-Nissan mixing behavior. This is consistent with the viscosity data, as

conductivities are usually found to be approximately inversely proportional to viscosities in ILs.[1, 102-104]

The density (figure 4, black squares) and molar volumes of the $[C_2mim]_{1-x}[C_{12}mim]_x[Tf_2N]$

mixture system exhibit smaller deviations from ideal mixing behavior (using a linear mixing law as

shown in equation 3) than the viscosity and conductivity. The observed densities are lower than

expected based on a linear mixing law and the maximum deviation occurs at around $x = 0.5$. Excess

molar volumes calculated from the density data are somewhat scattered (figure 4, red circles),

probably because they represent very small differences and any small errors in the measured densities

are magnified, and do not show a particularly clear trend across the composition range. However,

there is a tendency for small, positive excess molar volumes in these mixtures.
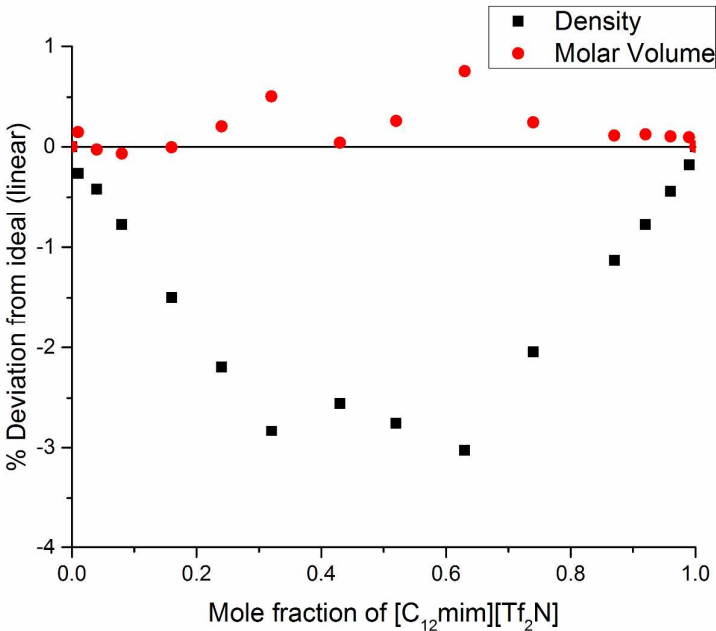
Figure 4: Percentage deviation of density and molar volume (at 293 K) from ideal behavior modelled

using a linear mixing law for $[C_2mim]_{1-x}[C_{12}mim]_x[Tf_2N]$ mixtures as a function of composition. Note

that error bars are included but are not visible as they are very small.

Small-angle X-ray scattering measurements

SAXS measurements have been shown in a range of studies to give good insight into the

nanostructure present in pure ILs.[105-119] In order to further probe the bulk structure of $[C_2mim]_{1-x}[C_{12}mim]_x[Tf_2N]$ mixtures, SAXS measurements were performed on 16 compositions from $x = 0$ to $x = 1$ at 301 K (figure 5).
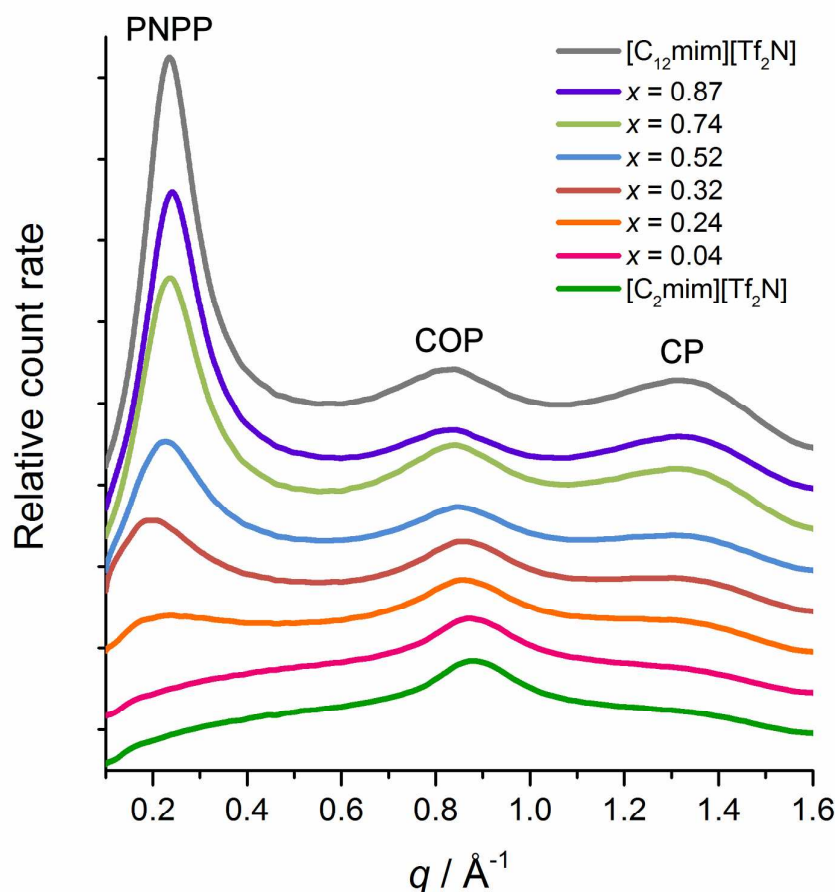
Figure 5: Selected SAXS data at 301 K for $[C_2mim]_{1-x}[C_{12}mim]_x[Tf_2N]$ mixtures as a function of composition. Data have been smoothed and stacked using an arbitrary offset on the y-axis to improve legibility and the PNPP, COP and CP peaks are labelled (see main text for descriptions). Data including all compositions can be found in the ESI.

Three peaks are often seen in SAXS data for ILs. These can be assigned to i) the characteristic distances between ions of different charge at close-contact (contact peak, CP) at high q (~1.3 $Å^{-1}$); ii) characteristic distances related to the alternation of ions within the polar network of the IL (charge-ordering peak, COP) (~0.8-0.9 $Å^{-1}$); and iii) characteristic separations caused by the segregation of polar and non-polar domains within the IL (polar/non-polar peak, PNPP) at low q (~0.2-0.25 $Å^{-1}$).[120-121] In pure $[C_2mim][Tf_2N]$ only the COP is clearly visible, although there is a suggestion of a broad CP, which has been identified by others for this IL.[113, 120] This is consistent with the fact that $[C_2mim][Tf_2N]$ does not form a nanostructured liquid. In contrast, in pure

10

[C_{12}mim][Tf_2N] the PNPP is clearly visible and this is indicative of nanoscale organization within the liquid, with the PNPP indicating the formation, and length scale, of local bilayer structure formed by the separation of the polar parts of the IL by the non-polar C12 chains on the cation. In the case of [C_{12}mim][Tf_2N], MD simulations suggest that this nanostructure can be identified as a bicontinuous network of polar and non-polar domains that percolates through the IL.[120]

What has been discovered here is that in [C_2mim]$_{1-x}$[C_{12}mim]$_x$[Tf_2N] mixtures the PNPP begins to appear as an incipient peak at 24 mol% [C_{12}mim][Tf_2N] and, as the concentration of [C_{12}mim][Tf_2N] increases it gains in intensity, sharpens and moves to higher q (from ~0.20 to 0.24 Å^{-1}, representing length scales of ~31 to 26 Å, respectively). The COP changes little in intensity with composition, but its position shifts slightly, representing an increase of around 5.5%, from 7.1 Å in pure [C_2mim][Tf_2N] to 7.5 Å in pure [C_{12}mim][Tf_2N]. Finally, the CP becomes more visible as the concentration of [C_{12}mim][Tf_2N] increases, although its position appears to vary little. These changes will be discussed further below in the context of our complementary neutron scattering results and MD simulations, and compared to data obtained for a series of pure [$C_n$mim][Tf_2N] ILs for $2 \leq n \leq 10$.[120]

Small-angle neutron scattering measurements

In order to gain additional insight into the structure of the bulk phase, SANS measurements were performed on the [C_2mim-d_{11}]$_{1-x}$[C_{12}mim]$_x$[Tf_2N] system; data for seven compositions ($x = 0.04$, 0.24, 0.32, 0.52, 0.74, 0.87 and 1) are presented here. Data were collected on the D22 small-angle diffractometer at the Institut Laue-Langevin (ILL) in Grenoble. Perdeuterated [C_2mim-d_{11}][Tf_2N] was used to give contrast between the [C_2mim]$^+$ and [C_{12}mim]$^+$ ions in the mixtures, as protonated and deuterated species typically have very different neutron scattering length densities (SLDs). Data were collected over a q-range of *ca.* 0.01 to 0.9 Å^{-1}, which corresponds to length scales of *ca.* 630 to 7 Å. Full details of the synthetic procedure used to prepare [C_2mim-d_{11}][Tf_2N] and SANS experimental details are given in the ESI.
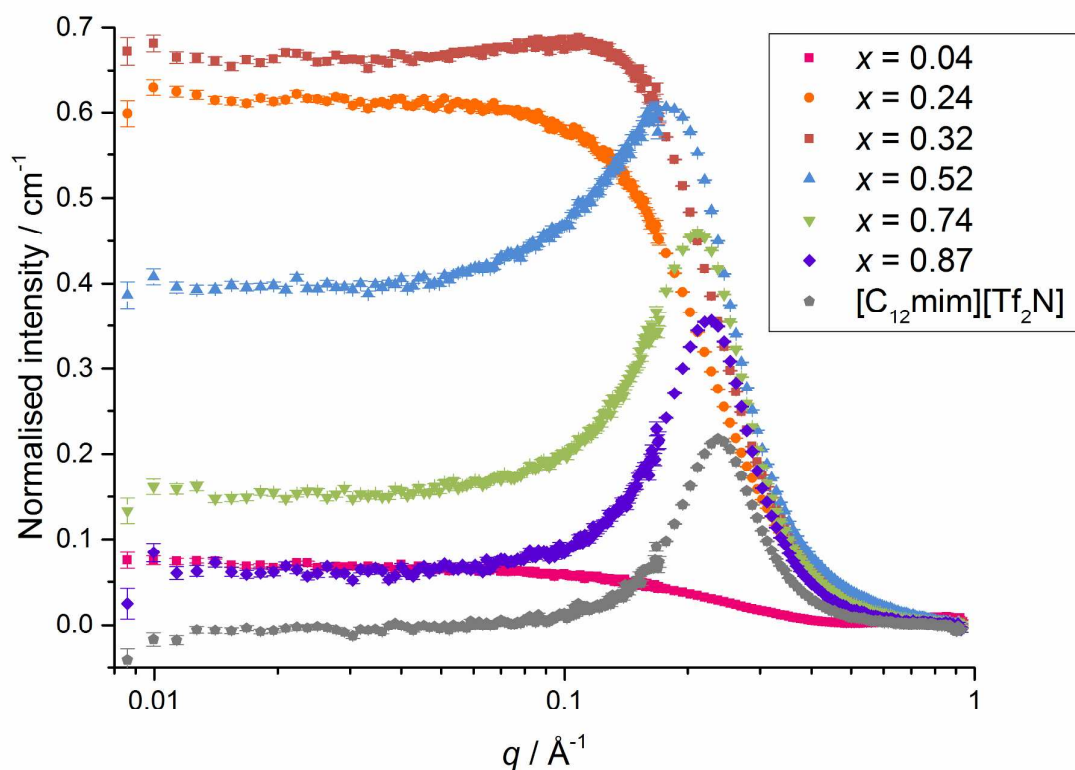
Figure 6: SANS data for $[C_2mim\text{-}d_{11}]_{1\text{-}x}[C_{12}mim]_x[Tf_2N]$ mixtures as a function of composition. Data are normalized to the background values determined during data fitting.

The SANS data in figure 6 show clear differences in neutron scattering as a function of composition. At lower loadings of $[C_{12}mim][Tf_2N]$ in $[C_2mim\text{-}d_{11}][Tf_2N]$ (4 and 24 mol% $[C_{12}mim][Tf_2N]$) the scattering intensity decreases relatively smoothly with increasing q. However, the data for the mixtures containing 52, 74 and 87 mol% $[C_{12}mim][Tf_2N]$ are dominated by a large peak between $ca.$ 0.2 and 0.25 Å^{-1}, which is also visible in the data at 32 mol% $[C_{12}mim][Tf_2N]$. This peak corresponds to the PNPP peak seen in the SAXS data.

The SANS data suggest a picture that is qualitatively similar to that obtained from the SAXS data, in that the PNPP appears in the data between 24 and 32 mol% $[C_{12}mim][Tf_2N]$. However, a more detailed picture can be obtained from the SANS data by fitting to scattering models; two different models have been employed. An ellipsoidal model describes a system composed of ellipsoidal scattering aggregates with a particular SLD (in this case the approximate SLD of non-

deuterated alkyl chains, -3.7×10^{-7} Å^{-2}) dispersed within a solvent with a particular SLD (in this case

the SLD of the [C$_2$mim-d_{11}][Tf$_2$N] and cationic head groups of the [C$_{12}$mim]$^+$ ions, which depends on

the composition of the mixture). The ellipsoids are characterized by axial and equatorial radii, and the

volume fraction of the system that they occupy. At low loadings of [C$_{12}$mim][Tf$_2$N] (4 and 24 mol%)

the ellipsoidal model fits the data quite well (see ESI for fits), although the fit is poorer at 24 mol%.

This is potentially because an incipient PNPP at this composition changes the form of the scattering

data without being obvious as a peak, due to the low q scattering that is present. The ellipsoidal model

does not fit the data at $x \geq 0.32$.

The Teubner-Strey model, which has the following form, can be used to fit the data across all

compositions (see ESI).[122-123]

$$I(q) = \frac{1}{a + c_1 q^2 + c_2 q^4} + background \quad (4)$$

where a, c_1 and c_2 are empirical fitting parameters that can be related to three quantities of interest by

the following relationships:

$$d\text{-}spacing = \frac{2\pi}{\sqrt{\frac{1}{2}\sqrt{\frac{a}{c_2}} - \frac{1}{4}\frac{c_1}{c_2}}} \quad (5)$$

$$correlation\ length = \frac{1}{\sqrt{\frac{1}{2}\sqrt{\frac{a}{c_2}} + \frac{1}{4}\frac{c_1}{c_2}}} \quad (6)$$

$$\gamma(amphiphile\ strength) = \frac{c_1}{\sqrt{4ac_2}} \quad (7)$$

The Teubner-Strey model is often used to describe systems that undergo a transition between discrete

aggregates (or micelles) and a bicontinuous network as a function of composition (*e.g.*

microemulsions).[122-123] The model fits the data well at low [C$_{12}$mim][Tf$_2$N] loadings, also reproducing

the key features of the data at higher mole fractions of [C$_{12}$mim][Tf$_2$N] in the mixtures. These two

models give complementary information about the system and the fitting parameters that were used

are summarized in table 1.

Table 1: Fitting parameters for an ellipsoid model of the SANS data for $[C_2mim-d_{11}]_{1-x}[C_{12}mim]_x[Tf_2N]$ mixtures ($x = 0.04$ and 0.24) and derived parameters for the Teubner-Strey model of the SANS data for all $[C_2mim-d_{11}]_{1-x}[C_{12}mim]_x[Tf_2N]$ mixtures.

IL system	Ellipsoid model				Teubner-Strey model		
	Axial radius (Å)	Equatorial radius (Å)	Volume fraction occupied by ellipsoidal scatterers	Theoretical volume fraction occupied by C12 chains	d-spacing (Å)	Correlation length (Å)	Amphiphile strength, γ
$x = 0.04$	12(1)	65(1)	0.01(1)	0.03	42	5	0.3
$x = 0.24$	15(1)	6(1)	0.16(1)	0.14	40	6	0.1
$x = 0.32$	-	-	-	0.18	37	7	–0.1
$x = 0.52$	-	-	-	0.26	30	9	–0.5
$x = 0.74$	-	-	-	0.34	27	12	–0.8
$x = 0.87$	-	-	-	0.38	26	13	–0.8
$x = 1$	-	-	-	0.41	25	16	–0.9

At 4 and 24 mol% $[C_{12}mim][Tf_2N]$, when the ellipsoid model can be used to fit the data, the scattering ellipsoids are found to be prolate and their dimensions correspond to approximately two or three C12 chains (an extended C12 chain is ~ 16 Å long) that interdigitate slightly. As expected, the volume fraction of the system occupied by the aggregated C12 alkyl chains increases with mole fraction of $[C_{12}mim][Tf_2N]$ in the mixture. Those in the fitting model can be compared with a theoretical value calculated from the approximate volumes of the non-polar parts of the C12 alkyl chains and the polar parts of the system (the cationic head groups, including alkyl carbon atoms connected directly to nitrogen and the anions) assessed using a group-contribution model described previously.[124-126] There is good agreement between the volume fractions used in the fitting model at 24 mol% $[C_{12}mim][Tf_2N]$, but the fitted value is somewhat low at 4 mol% $[C_{12}mim][Tf_2N]$, which may be due to the presence of isolated C12 chains in this mixture that may not contribute significantly to the observed neutron scattering.

The Teubner-Strey model allows the extraction of the 'amphiphile strength' parameter (γ): typically for $\gamma > 1$ the system is regarded as disordered, aggregate/micelle formation is seen for $0 < \gamma < 1$, bicontinuous structures are found where $-1 < \gamma < 0$ and lamellar structures are seen when $\gamma < -1$. As the SANS data for the $[C_2mim-d_{11}]_{1-x}[C_{12}mim]_x[Tf_2N]$ mixtures are quite well described by the Teubner-Strey model (see ESI for fits), the γ parameter for these mixtures can be interpreted in the same way to give a picture of the structure in the bulk. For mixtures containing 4 and 24 mol%

14

[C$_{12}$mim][Tf$_2$N], $0 < \gamma < 1$ suggesting that isolated aggregates of C12 chains from the [C$_{12}$mim]$^+$ ion

exist. This is consistent with the fact that the SANS data for these compositions can also be fitted to a

model based on ellipsoidal scattering objects. By 32 mol% [C$_{12}$mim][Tf$_2$N], γ has become just

negative and decreases in value steadily as the amount of [C$_{12}$mim][Tf$_2$N] in the mixture increases,

ultimately reaching a value of −0.9 for pure [C$_{12}$mim][Tf$_2$N]. This suggests a change in structure from

isolated aggregates of C12 chains to a bicontinuous network of non-polar and polar domains within

the ILs as a function of composition.

At compositions where $x < 0.32$, the d-spacing (which can be interpreted as the average

distance between scattering objects) decreases with increasing amounts of [C$_{12}$mim][Tf$_2$N] in the

mixture, as one would expect with an increasing concentration of long alkyl chains and thus an

increase in the aggregate density. As the amount of [C$_{12}$mim][Tf$_2$N] in the mixture increases, and the

structure switches from isolated aggregates to form a continuous non-polar sub-phase, there is a large

decrease in d-spacing (from 40 to 30 Å between 24 and 52 mol% [C$_{12}$mim][Tf$_2$N]). The d-spacing

then decreases steadily with increasing mole fraction of [C$_{12}$mim][Tf$_2$N] in the mixture to 25 Å in the

pure IL. Within this regime, the d-spacing is derived from the position of the PNPP, as in the SAXS

data, and can be interpreted in the same way $i.e.$ as the length scale of local bilayer structures formed

from the C12 alkyl chains.

Molecular dynamics simulations of the bulk

In order to better understand the bulk structure of this system and to aid interpretation of the

SANS/SAXS data, molecular dynamics (MD) simulations were performed on [C$_2$mim]$_{1-}$

$_x$[C$_{12}$mim]$_x$[Tf$_2$N] mixtures, where x = 0, 0.04, 0.24, 0.32, 0.52, 0.74, 0.87 and 1, matching

compositions studied $in\ vitro$. Condensed-phase MD simulations were carried out using the DLPOLY

package.[127] All molecules were modeled using the CL&P atomistic force field,[128-129] which is based on

the OPLS-AA framework [130] but was to a large extent developed specifically for encompassing entire

homologous series of ionic liquids. Due to the slow dynamics of this type of system, special care was

taken to ensure the attainment of equilibrium conditions: (i) equilibrations started from initial low

density configurations, with ions placed randomly in periodic cubic boxes; (ii) typical equilibrations

were implemented for more than 1 ns; (iii) multiple re-equilibrations through the use of temperature

annealing and switching off and on of the Coulomb interactions were performed; (iv) further

simulation runs were used to produce equilibrated systems at the studied temperatures. The

equilibrated systems were used in production runs of at least 4 ns at 500 K (see ESI for details).The

simulations were performed at 500 K to improve the dynamics and equilibration of the simulated

systems. Nonetheless, comparisons between the main structural features of systems simulated at 500K

and 300K are possible, as proven by the green and grey lines in figures 6(a) and 6(b), corresponding

to pure $[C_2mim][Tf_2N]$ and $[C_{12}mim][Tf_2N]$ at the two temperatures (*vide infra*). The simulations

allow structure factor functions, $S(q)$, to be calculated for each IL (shown in figure 7). The structural

analysis has focused on the low-q region of the $S(q)$ functions ($0.2 < q/\text{Å}^{-1} < 1.8$). In that range most

ionic liquids feature three peaks, the CP, COP and PNPP, as described above. These can be compared

to the SAXS data presented above, with which they are in excellent agreement, giving confidence in

the robustness of the computational methodology. In addition, the MD trajectories can be analyzed to

provide a more detailed understanding of the aggregation and structural characteristics of the ILs

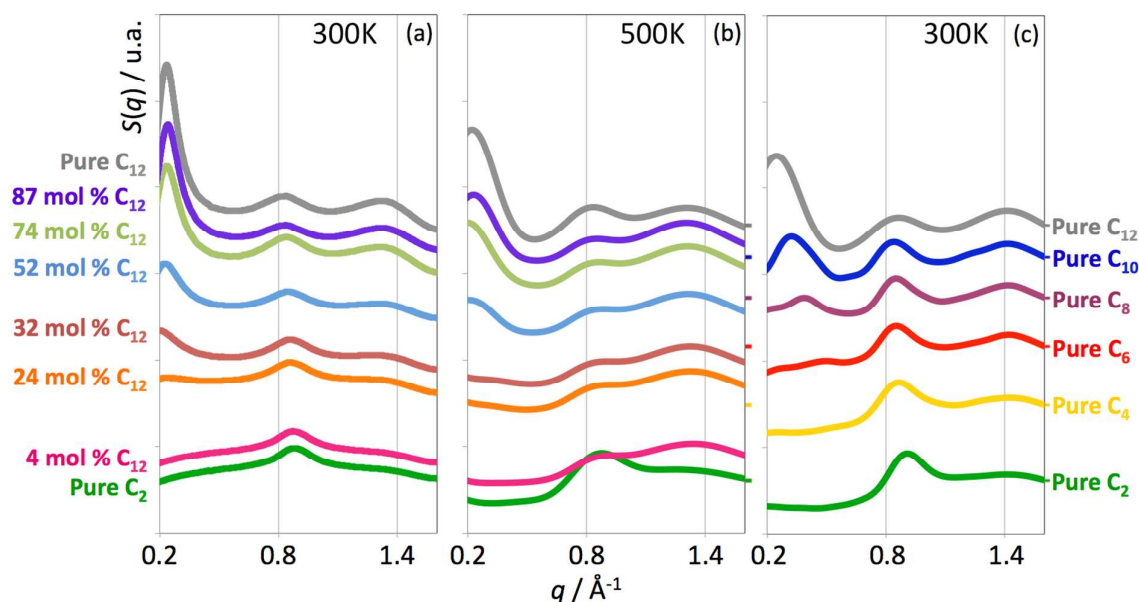under study (discussed in detail below).

Figure 7: (a) Experimental SAXS data for $[C_2mim][Tf_2N]$, $[C_{12}mim][Tf_2N]$ and selected $[C_2mim]_{1-}$

$_x[C_{12}mim]_x[Tf_2N]$ mixtures. (b) Calculated total structure factor functions, $S(q)$ for the same ILs and

IL mixtures at 500 K. (c) Calculated $S(q)$ functions of six pure $[C_nmim][Tf_2N]$ ionic liquids at 300

K.[119, 126] All $S(q)$ functions were shifted, in proportion to the volume fraction of the liquid occupied by

the non-polar alkyl chains, in the y-axis direction in order to improve legibility. Shifting the data in

this way also allows the IL mixtures to be compared to the pure ILs (see text for details and also note

the position of the colored markers on the right hand side of the middle graph).

Figure 7b shows the structure factor functions, $S(q)$, for the IL mixtures in this study and 6c

shows $S(q)$ functions of six pure ionic liquids (all even-numbered chains from $[C_2mim][Tf_2N]$ to

$[C_{12}mim][Tf_2N]$) at 300 K.[97, 120] Also shown for comparison (figure 7a) are experimental SAXS data

collected as part of this study (*vide supra*). A comparison of the experimental SAXS data and

calculated $S(q)$ functions for the IL mixtures shows good agreement between experiment and theory.

In both sets of data, the PNPP begins to appear as an incipient peak at $x = 0.32$, which grows in

intensity and shifts to higher q with increasing mole fraction of $[C_{12}mim][Tf_2N]$. In the case of the

MD simulations, the incipient PNPPs in the 24 to 32 mol% regions are difficult to ascertain due to the

impossibility of calculating data below q-values of 0.2 Å^{-1} in the simulations, due to finite-size effects

of the simulation boxes. In addition, the COP shifts steadily to lower q with increasing mole fraction

of $[C_{12}mim][Tf_2N]$. A comparison of the $[C_2mim][Tf_2N]$ and $[C_{12}mim][Tf_2N]$ pure ionic liquids at 300

and 500 K (green and grey lines in figures 6b and 6c) shows that the $S(q)$ differences between the two

simulation temperatures are small (COPs and CPs become less pronounced at higher temperatures).

Thus, it is possible to make a comparison between the IL mixtures and pure ILs simulated at the two

temperatures.

It was shown in previous work[57, 131] that the volumetric behavior of IL mixtures is additive

and almost ideal: that means that at a given temperature, the volume occupied by an ion in an ionic

liquid is almost constant, regardless of the counter-ion. Indeed, the fact that densities only deviate

very slightly from ideal mixing behavior in the system under study here (figure 4) suggests that this is

true in these IL mixtures. This notion supports the use of group-contribution rules to estimate the molar volume of ionic liquids. Likewise, the contribution of the alkyl side chains to the molar volume of an ion is also additive and constant: each methylene -CH_2- group added to a chain at 298 K increases the molar volume of the ion by around 17 cm^3 mol^{-1}. This suggests that a comparison can be made between different ILs (pure or mixtures) based on the volumes occupied by the polar network and the non-polar domains. For instance, an equimolar ($[C_2mim][Tf_2N] + [C_{12}mim][Tf_2N]$) mixture has around the same non-polar volume fraction as pure $[C_7mim][Tf_2N]$, 4 mol% $[C_{12}mim][Tf_2N]$ has a non-polar volume fraction in-between that of $[C_2mim][Tf_2N]$ and $[C_3mim][Tf_2N]$ and so on. A comparison of the mixtures and pure ILs shows the following revealing similarities and differences:

i) the PNPP and CP intensity trends in the mixtures are similar to those observed for the pure ionic liquids, *i.e.*, both increase for systems with long-chain cations. The intensities of the PNPPs are higher and are found at a lower q-value (see point ii) in the mixtures than in pure ionic liquids with similar non-polar volume fractions. As in the SAXS data, PNPPs start to emerge as an incipient peak in the 24 mol% $[C_{12}mim][Tf_2N]$ mixture and between the pure ILs $[C_4mim][Tf_2N]$ and $[C_6mim][Tf_2N]$, and grow in intensity either with increasing mole fraction of $[C_{12}mim][Tf_2N]$ in the mixture or with increasing chain length in the pure ILs. Thus, there is some correlation between the appearance, and growth in intensity, of the PNPP and the non-polar volume-fraction of the liquid, regardless of whether or not this was achieved through mixing or by increasing chain length on the cation. This correlation is striking for the $[C_2mim]_{1-x}[C_{12}mim]_x[Tf_2N]$ mixtures investigated here, but more work would be needed on related systems to establish whether it is a generally causal effect.

ii) the PNPP peak positions shift substantially to lower q with increasing chain length in the pure ILs, corresponding to an increase in length scale of the non-polar network with increasing chain length. However, the PNPP position in the mixtures is much less sensitive to composition, and shifts in the opposite direction, to higher q with increasing mole fraction of $[C_{12}mim][Tf_2N]$ (from ~32 to 26 Å). This origin of this shift is discussed below. Thus, the q-values of the PNPPs are controlled predominantly by the longest chains present in the systems, since these dictate the length scale of the non-polar network. Thus, in structural terms, the mixtures do not behave as though they were single components with a chain length that is an average determined by composition.

18

iii) the COP intensities (relative to the CP intensities) are depressed in the case of the

mixtures. Moreover, the COP intensity increases slightly in mixtures containing a larger proportion of

$[C_{12}mim][Tf_2N]$, whereas it decreases for pure ILs with increasing cation chain length. The less

structured polar network of the mixtures may be related to the existence of isolated C2 moieties that

perturb its organization.

iv) in both the SAXS data and MD simulations, the COP positions in the $S(q)$ functions shift

monotonically to lower q-values both in the mixtures and in the pure ILs. It was found previously,[97,]

[120-121, 132-134] that such a trend is related to the stretching of the polar network as it has to accommodate

larger non-polar domains in its midst.

The MD trajectories were analyzed carefully to establish the different aggregation patterns

that are possible within the non-polar domains that constitute the different systems.[120-121] Figure 8

shows the tail-tail aggregation distributions in the mixtures. In this figure, the probability of finding a

chain belonging to an aggregate of a particular size is given on the y-axis, and the aggregate size is

given on the x-axis.
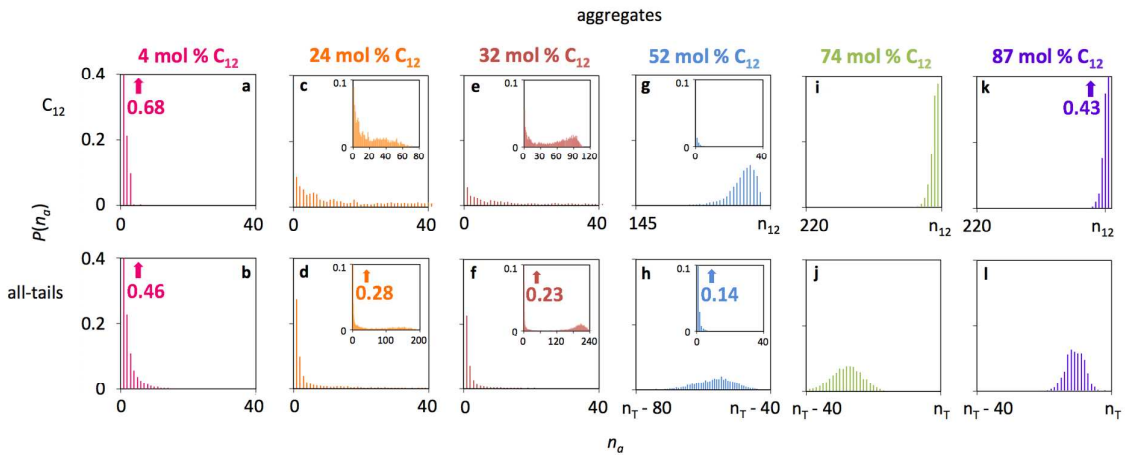
Figure 8: Discrete probability distribution function, $P(n_a)$, of a given chain belonging to a non-polar

aggregate of size n_a. Aggregates of only C12 chains are shown in the top panels (a, c, e, g, i and k)

and aggregates containing both C12 and C2 chains are shown in the bottom panels (b, d, f, h, j and l).

All y-axes are on the same (probability) scale, but different x-axes (and selected inserts) are used to

highlight the key information. 'n_{12}' and 'n_T' represent the total number of C12 and (C2 + C12) chains

present in the mixtures, respectively. The numbers and arrows in the text correspond to out-of-the-scale values, e.g. in 7a $P(n_a=1) = 68\%$ i.e. 68% of the C12 chains are isolated; $P(n_a=2) = 21\%$ i.e. 21% of the C12 chains form "C12 dimers"; $P(n_a=3) = 8\%$ i.e. 8% of the C12 chains form "C12 trimers".

The first composition (4 mol% $[C_{12}mim][Tf_2N]$) of figure 8a and 8b shows that the aggregates formed by only dodecyl or both chains are always quite small (aggregates of ethyl chains from $[C_2mim]^+$ are small at all compositions, see ESI for details). On moving to the second composition (24 mol% $[C_{12}mim][Tf_2N]$) the mixture exhibits more interconnected, non-polar domains and the light orange bar distribution in figure 8c shows the existence of large aggregates of C12 chains, which nevertheless never contain all (350) of the dodecyl chains present in the system. Due to their length, the majority of dodecyl chains are in contact with other dodecyl chains (only about 10% are isolated). However, ethyl chains from the $[C_2mim]^+$ ion essentially do not aggregate, as would be expected from this essentially non-amphiphilic ion and around 67% of the ethyl chains are completely isolated (see ESI). The next composition (32 mol% $[C_{12}mim][Tf_2N]$) is much closer to the percolation limit of the alkyl side chains contained in the box. In fact, figures 7e and 7f show that the probability of C12 chains belonging to very large aggregates is already greater than that corresponding to the inclusion in smaller aggregates (a bump starts to develop on the right-hand side of the histograms). The other mixtures (figures 7g to 7l) show non-polar domains formed by large, percolating clusters of the long chains, which can be described as being 'decorated' by ethyl chains from $[C_2mim]^+$ ions. In these last mixtures, the ethyl chains that are not connected to the dodecyl moieties become more and more isolated from each other (ethyl-only clusters become scarcer, see ESI).
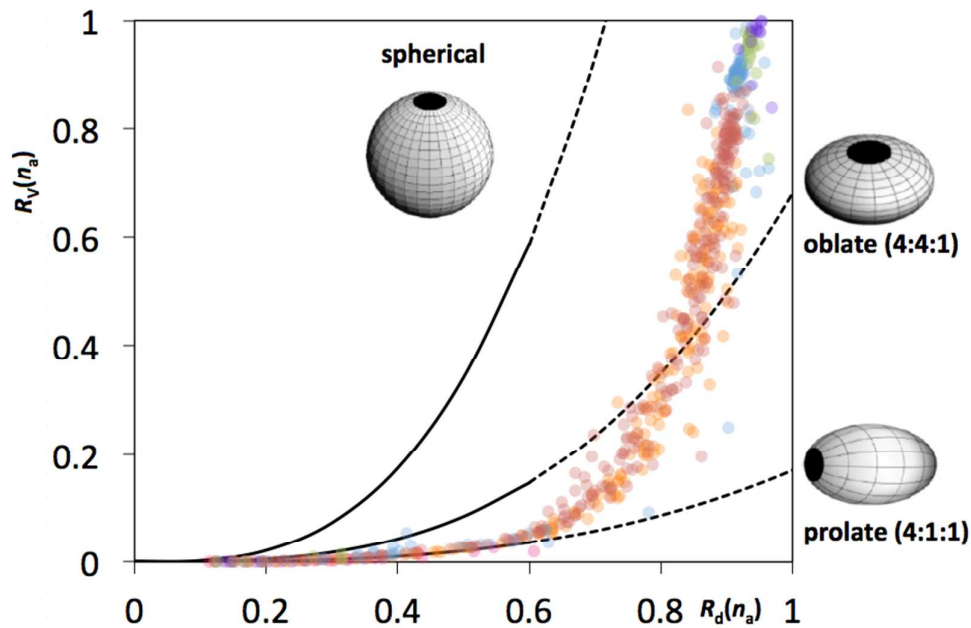
Figure 9: Aggregate volume-to-box volume ratio, $R_V(n_a)$, as a function of maximum aggregate length-to-box-diagonal ratio, $R_d(n_a)$ for all chains aggregates in the mixture series. The black guidelines represent the volume-to-maximum-length ratios for spheres, oblate ellipsoids and prolate ellipsoids in order to guide the eye.

Figure 9 shows the relationship between the length and volume of the tail aggregates – a measure of their shapes – as their sizes become progressively larger (from the lower left to the upper right corners of the graphs). It shows that the shape of the aggregate is more or less independent of the type of chains it contains, but strongly dependent on its size: small aggregates have a prolate shape that evolves gradually as their size increases to more globular structures, perhaps best viewed as fragments of a non-polar network, which eventually coalesce and percolate throughout the system. This is consistent with the SANS modelling, where prolate ellipsoidal scattering objects fit the data reasonably well at low mole fractions of $[C_{12}mim][Tf_2N]$ in the mixtures and the system is described as a bicontinuous network of polar and non-polar domains when more $[C_{12}mim][Tf_2N]$ is present.

Figure 10: (a – c) Average size of contact neighbors, N_i, in the chain aggregates (filled color circles) as a function of the non-polar volume fraction of the liquids plotted as the x-axis. (a) ethyl aggregates; (b) dodecyl aggregates; (c) all non-polar aggregates.

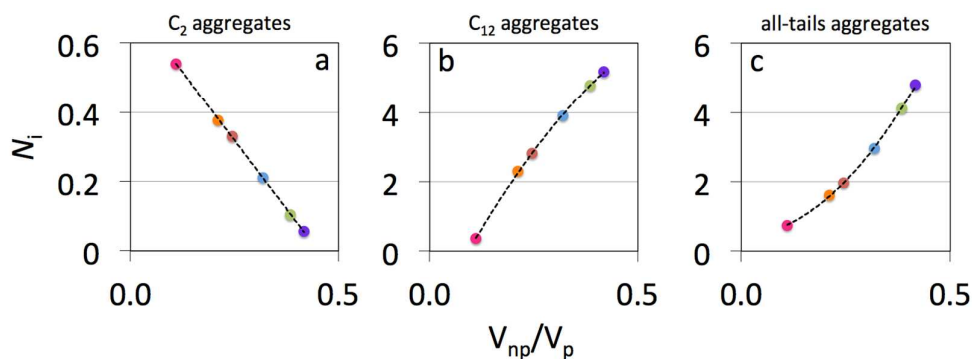The aggregation analysis can also calculate the average number of direct contact neighbors (other chains) that a given side chain may have within the non-polar domains (figure 10). The number of neighbors depends strongly on the size of the chains, since longer chains have more potential contact points, and their degree of aggregation. Figures 9b and 9c show that as the non-polar volume fraction of the liquid increases (with increasing $[C_{12}mim][Tf_2N]$ mole fraction) the number of nearest neighbors increases, which is similar to the trends observed for pure ILs with increasing alkyl chain length.[134] The ethyl chains show different behavior (figure 10a). These chains have very low average neighbor numbers, observed values below 1 denote a large proportion of isolated ethyl chains, and the number of neighbors decreases with increasing non-polar volume fraction. Thus, as in the pure IL $[C_2mim][Tf_2N]$ (figure 2, left), the ethyl chains of the $[C_2mim]^+$ ion in these mixtures are not strongly organized and are predominantly found as isolated ethyl chains distributed throughout the IL.

RAS-LIF experiments

As in our previous work on IL surface structure,[83, 87, 93-94, 135-136] RAS-LIF experiments were used to probe the vacuum-liquid interface in $[C_2mim]_{1-x}[C_{12}mim]_x[Tf_2N]$ mixtures, where $x = 0, 0.01, 0.04,$

0.08, 0.16, 0.24, 0.52, 0.74, 0.87 and 1 (see ESI for experimental details). RAS-LIF is a very surface-sensitive technique that aims to detect selectively the abstractable hydrogen atoms exposed at the surface of an IL by reaction with gas-phase O(^{3}P) atoms.[83, 137] This produces OH radicals that scatter back into the gas phase, where they are detected by laser-induced fluorescence (LIF). The translational energy distribution of the incident O(^{3}P) atoms is such that a significant fraction of the O(^{3}P) atoms are capable of abstracting an H atom from weaker, 2° C-H bonds, but not from stronger C-H bonds.[83, 136] Consequently, the detection of CH$_2$ groups in the alkyl chains is strongly favored over other types of H, including those in the CH$_3$ groups or attached to the imidazolium ring. Thus, interfacial reactivity observed in a RAS-LIF experiment is a quantitative measure of the accessibility of these CH$_2$ groups at the surface.

The rotational distributions of the OH products were characterized by recording LIF excitation spectra at a fixed delay between the photolysis and probe laser pulses in order to confirm that the distributions did not vary materially across the range of mixtures. This was indeed the case as described in detail in the ESI. The LIF intensity of a single transition could, therefore, be taken to be representative of the total number density of OH scattered from the surface.

Appearance profiles (the LIF intensity as a function of delay between photolysis and probe lasers) were measured on the most intense line in the spectrum corresponding to the Q$_1$(1) transition. Details of the procedure and the correction for minor background signals are given in the ESI. The resulting profiles for the pure ILs, selected mixtures and the squalane reference are presented in figure 11. Consistent with our previous results,[83 87, 93-94] the OH yield from [C$_2$mim][Tf$_2$N] is almost below the measurable level while the [C$_{12}$mim][Tf$_2$N] surface has slightly more than half the reactivity of squalane. The yield of OH increases rapidly with x, showing significant reactivity for x of just 0.01. At $x \geq 0.24$, the profiles start to cluster together as they converge towards pure [C$_{12}$mim][Tf$_2$N].
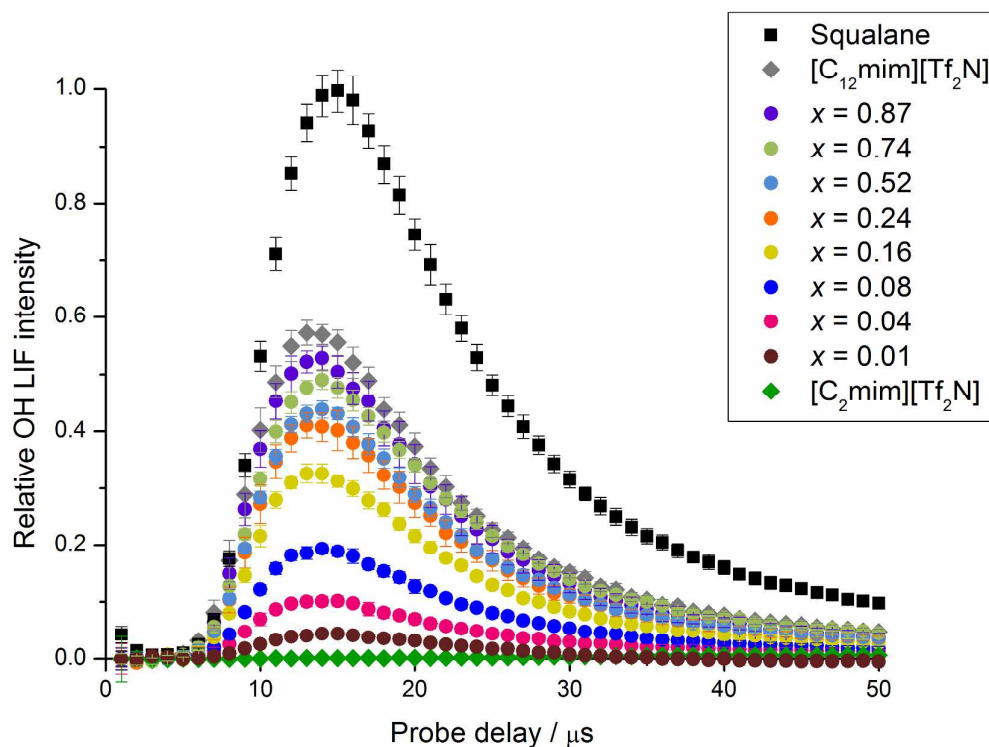
Figure 11: Selected OH appearance profiles for the reference compound squalane (black squares), against which all signals are normalised, $[C_{12}mim][Tf_2N]$ (grey diamonds), $[C_2mim][Tf_2N]$ (green diamonds) and representative $[C_2mim]_{1-x}[C_{12}mim]_x[Tf_2N]$ mixtures (circles, color code in figure). Each profile is an average of three independent sets of ten profiles each as described in the text. Error bars are 1σ standard error of the mean.

Relative values of reactivity were obtained from the appearance profiles by performing a density-to-flux transformation and integrating the resulting flux profiles between 0 and 30 µs, as described previously.[83] The resulting values are tabulated in the ESI (Table S5) and are plotted against mole fraction in figure 12a, where they are expressed as a fraction of the yield from pure $[C_{12}mim][Tf_2N]$. To allow a straightforward visual assessment of the departure from stoichiometry, a diagonal line has been included connecting the yields from pure $[C_2mim][Tf_2N]$ and $[C_{12}mim][Tf_2N]$, respectively (i.e. between the points with $x = 0$ and 1). To the extent that mole fractions represent the proportions of the surface occupied by different ions correctly, this straight line corresponds to stoichiometric behavior. It is clear that on this basis the RAS-LIF experiments find that the interfacial

reactivity is higher than the stoichiometric result across almost the full range. However, some care is needed here; it is questionable whether mole fraction is an unbiased independent variable against which to measure stoichiometric surface occupancy, simply because it does not recognize the different sizes of the two cation types. This point is explored quantitatively in the ESI, where two alternative versions of figure 12 are provided. These are constructed using as *x*-axis either the volume fraction (figure S50), calculated from the known relative molar volumes, V_m, of [C$_2$mim][Tf$_2$N] and [C$_{12}$mim][Tf$_2$N], or the area fraction (figure S51, taken to be proportional to $V_m^{2/3}$ (*i.e.* the cross-sectional area if the molecules were spherical). The positive deviations from stoichiometry remain clear in both of these plots. The choice of construction does not therefore change the qualitative conclusions, of which the principal one is that there is a clear, non-stoichiometric preference for the longer-chain [C$_{12}$mim]$^+$ cation to be exposed to attack at the surface at all concentrations except for the very richest mixtures with *x* close to 1.This is emphasized in figure 12b, which shows, on the same vertical and horizontal scales, the difference between the measured and stoichiometric values. The maximum deviation occurs in the vicinity of a mole fraction $x = 0.24$ (which, for comparison, is equivalent to a volume fraction of 0.34).
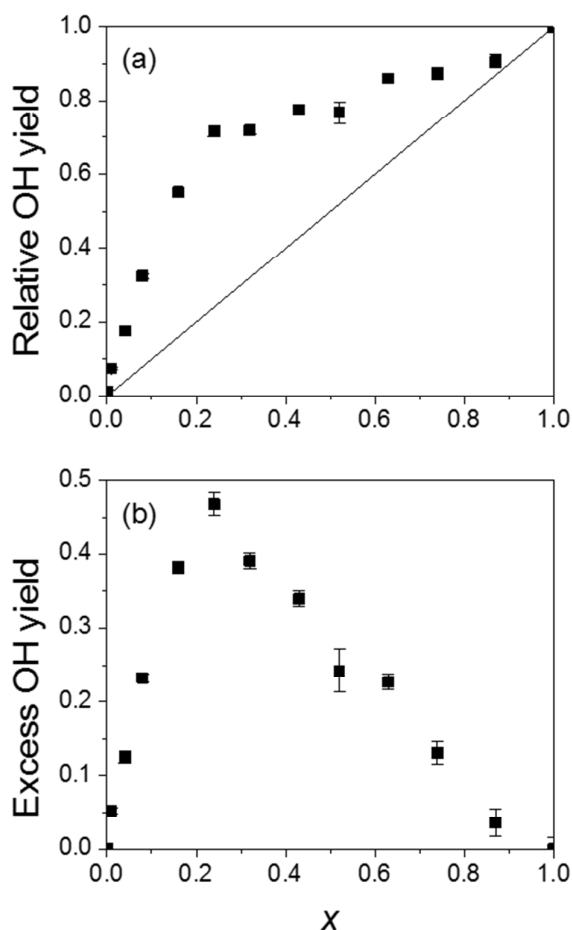
Figure 12: (a) Measured relative OH flux for $[C_2mim]_{1-x}[C_{12}mim]_x[Tf_2N]$ mixtures plotted against mole fraction of $[C_{12}mim]^+$. The diagonal line represents hypothetical stoichiometric behavior if the surface occupancy were simply proportional to mole fraction. (b) The difference between the experimental data points and the stoichiometric line.

Molecular dynamics simulations of the vacuum-IL interface

RAS-LIF vacuum-liquid scattering is ultimately controlled by the many-atom dynamics during and

after gaseous projectile collision with the vacuum-liquid interface. However, previous studies

demonstrate that liquid-dependent trends in RAS-LIF product flux can be qualitatively reproduced

with an analysis of static vacuum-liquid interface composition.[87, 135-136] To complement experiment, an

additional set of MD simulations were performed to model the vacuum-liquid interface of $[C_2mim]_{1-x}[C_{12}mim]_x[Tf_2N]$ mixtures (where $x = 0$, 0.04, 0.08, 0.16, 0.24, 0.52, 0.87 and 1) using the same

Lopes/Pádua all-atom, OPLS-type force field.[129, 138-142] Vacuum-liquid-vacuum slab structures were

prepared and subjected to 5 sequential equilibration cycles where each equilibration cycle consists of

a phase of elevated temperature (500 K) propagation followed by a phase of room-temperature (298

K) propagation. Data analysis was only performed on the final phase of room-temperature

propagation. Full simulation details are given in the ESI.
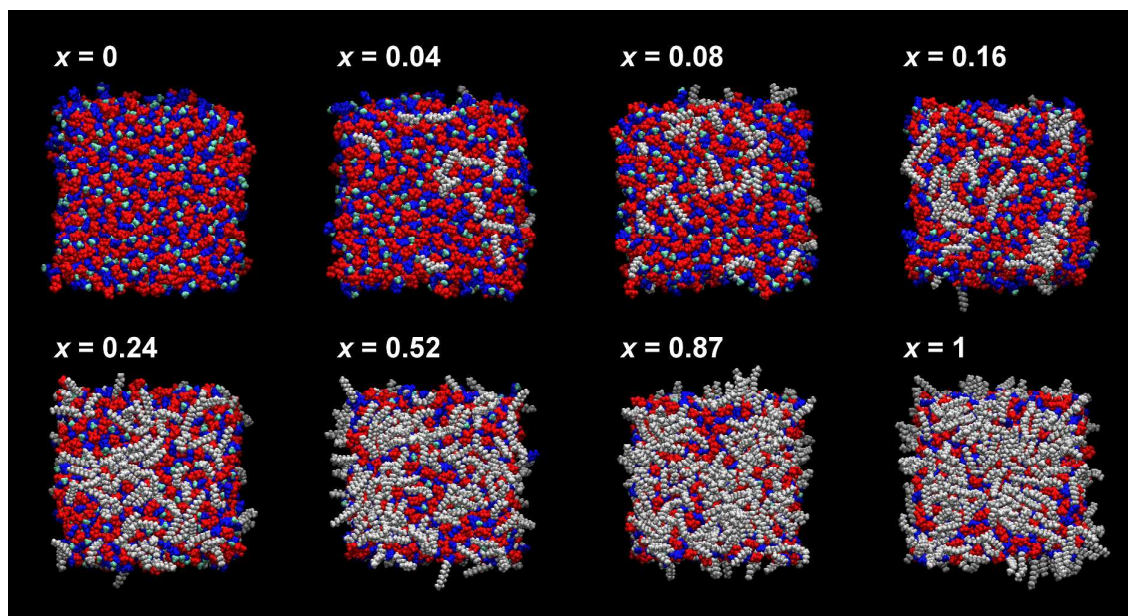
Figure 13: Top-down view of the vacuum-liquid interface of eight $[C_2mim]_{1-x}[C_{12}mim]_x[Tf_2N]$

mixtures where x=0, 0.04, 0.08, 0.16, 0.24, 0.52, 0.87, and 1. One periodic boundary condition unit

cell, referred to in the text as "unit cell", is shown for each liquid. Atoms associated with the $[Tf_2N]^-$

ion are colored red. The methyl group that terminates the ethyl chain in $[C_2mim]^+$ is colored green.

For $[C_2mim]^+$ and $[C_{12}mim]^+$ ions, the methyl substituent (4 atoms), imidazolium ring (8 atoms) and

the first methylene group of the alkyl substituent (3 atoms) are shown in blue. All other atoms of the

$[C_{12}mim]^+$ cation alkyl substituent are shown in grey.

Figure 13 is a compound image that displays the final trajectory frame of eight different $[C_2mim]_{1-x}[C_{12}mim]_x[Tf_2N]$ mixtures. Each frame presents a top-down view of the vacuum-liquid interface for a

single unit cell and liquid molecules are rendered as a collection of opaque, van der Waals spheres.

Accessible surface area (ASA) calculations were used to identify interfacial atoms and quantify cation

surface density (Figure 14a) and surface 2° hydrogen density (Figure 14b) as a function of

$[C_{12}mim][Tf_2N]$ mole fraction. Interfacial atoms are defined as all liquid atoms near the vacuum-

liquid interface that can accommodate contact with a 1.5 Å radius spherical probe.[83, 136] In figure 14c,

the excess surface 2° hydrogen density computed by ASA analysis of molecular dynamics data is

compared to the excess OH yield from RAS-LIF experiments. As described earlier, these excess

properties are derived by computing the deviation of the observed signal from hypothetical linear

behavior between pure $[C_2mim][Tf_2N]$ and pure $[C_{12}mim][Tf_2N]$ with x as a dependent variable. Note

that the excess properties in Figure 14c are computed from data normalized to the signal of pure

$[C_{12}mim][Tf_2N]$.

Since the nonpolar methyl group of $[C_2mim]^+$ (green in figure 13) is associated with 2 ethyl-

group methylene hydrogen atoms and the nonpolar undecyl group of $[C_{12}mim]^+$ (grey in figure 13) is

associated with 22 dodecyl-group methylene hydrogen atoms, figure 13 suggests that the total

methylene hydrogen atom density at the vacuum-liquid interface monotonically increases with x. This

is consistent with the experimental RAS-LIF data in figure 12a and the computed surface 2° hydrogen

density in figure 14b. The MD simulations show that this increase in 2° hydrogen atoms at the

vacuum-liquid interface is dominated by the $[C_{12}mim]^+$ dodecyl group at all mixture concentrations

studied. Due to the length of the dodecyl group, every surface-active $[C_{12}mim]^+$ cation adds a large

number of vacuum-accessible secondary hydrogen atoms. This increase in surface 2° hydrogen atoms

is most dramatic for mixtures with a low mole fraction of $[C_{12}mim][Tf_2N]$.

For pure [C$_2$mim][Tf$_2$N], the vacuum-liquid interface shows a strict pattern of alternating charged ion packing. As the mole fraction of [C$_{12}$mim][Tf$_2$N] increases from 0, the number density of [C$_2$mim]$^+$ at the vacuum-liquid interface decreases and the number density of [C$_{12}$mim]$^+$ at the vacuum-liquid interface increases (figure 14a). Figure 14a also demonstrates that the surface C12 mole fraction approaches 0.5 when the bulk mole fraction (approximated from the total system ion count) is ~0.16. Therefore, the C12 cation has a higher preference for the vacuum-liquid interface than the C2 cation. This observation is consistent with other studies of ionic liquid mixtures where, in general, larger ions are more surface active.[67, 86, 91-92] Comparing the excess OH yield from RAS-LIF experiments with the excess surface 2° hydrogen density from ASA analysis of MD simulations, excellent agreement is observed in the shape of the excess curve, the peak excess location, and the peak excess value (see figure 14c). Small modifications to the ASA parameters used to identify vacuum-accessible atoms do not change the peak excess position and only introduce small changes to the shape of the excess curve and the peak excess value. There are a number of possible technical reasons for the remaining small deviation between experiment including the simulation size and various limitations associated with the forcefield description of the liquid. However, the level of agreement is particularly striking because we reiterate that the correlation being drawn is between the RAS-LIF OH yield and the static vacuum-liquid interface composition as measured by a probe particle in the ASA analysis. This particle is not constrained to approach the surface only along trajectories that would lead to reaction of the corresponding O(^{3}P) atoms. The correspondence between experiment and simulation supports a correlation between RAS-LIF OH yield and the [C$_{12}$mim]$^+$ number density at the vacuum-liquid interface and provides validation of the vacuum-liquid interface predicted by classical molecular dynamics.
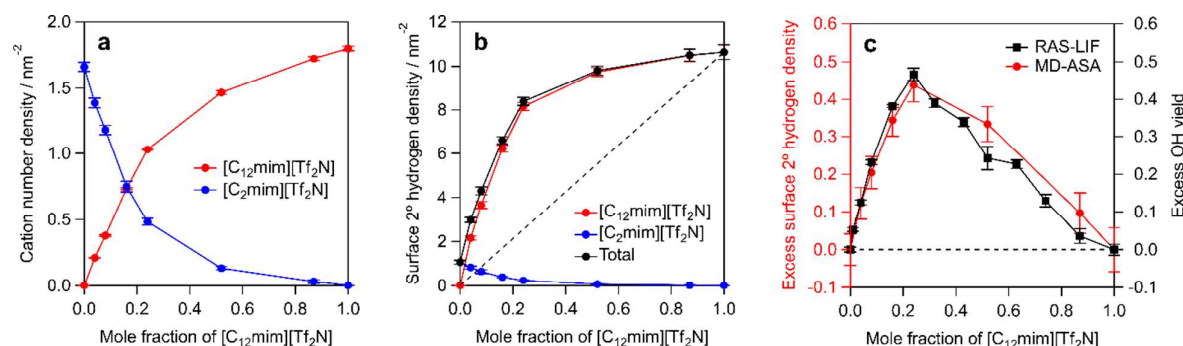
Figure 14: Surface structure and composition of $[C_2mim]_{1-x}[C_{12}mim]_x[Tf_2N]$ mixtures, as analyzed by accessible surface area (ASA) calculations. Surface area is defined by the x and y dimensions of the unit cell and does not account for corrugation of the liquid surface induced by capillary waves. The dashed diagonal line in panel b represents hypothetical linear or stoichiometric behavior between pure $[C_2mim][Tf_2N]$ and pure $[C_{12}mim][Tf_2N]$ as a function of total system mole fraction (see the discussion in the text relating to the construction of figure 12). In panel c, both experiment and simulation are normalized to the signal from pure $[C_{12}mim][Tf_2N]$ before computing the deviation from stoichiometric behavior. Error bars are $\pm 1\sigma$ standard error of the mean.

Discussion

A detailed molecular insight into the bulk-phase structure of the $[C_2mim]_{1-x}[C_{12}mim]_x[Tf_2N]$ system has been gained using a range of complementary techniques. This understanding allows a proposal to be made as to why the physical properties of this system change as they do with changing composition, and importantly to speculate on why some properties in this system deviate more strongly from ideal behavior than others.

Four key observations on the bulk properties in particular require explanation and they are considered in the discussion that follows:

1) The onset of significant deviation from ideal bulk physical property behavior occurs at around 24 mol% $[C_{12}mim][Tf_2N]$.

2) Viscosity data deviate more significantly from ideal mixing behavior than conductivity data, whereas densities show only small deviations from ideal behavior.

3) Observed viscosities are higher, and conductivities lower, in these mixtures than would be

    expected based on simple mixing laws.

4) Densities are slightly lower than ideal, and there is a slight tendency for small, positive excess

    molar volumes, in these mixtures.

The SAXS, SANS and MD simulations can now be brought together to give a consistent picture of the bulk-phase structure of the $[C_2mim]_{1-x}[C_{12}mim]_x[Tf_2N]$ mixtures. At low mole fractions of $[C_{12}mim][Tf_2N]$ (*e.g.* 4 mol%) only small aggregates (2-3 alkyl chains) of C12 chains are present in the liquid. The appearance of an incipient PNPP from 24 mol% $[C_{12}mim][Tf_2N]$ reflects the presence of some aggregates of C12 alkyl chains with a bilayer structure of sufficient size and coherence length to produce a PNPP. MD simulations suggest that although small aggregates are more common, aggregates with a range of sizes form at this composition, the largest containing ~17% of the C12 chains (see figure 8 for quantitative data regarding the number of alkyl chains found in aggregates at each composition). SANS fitting gives a slightly positive γ value, which agrees with the simulations that this structure is best described as isolated aggregates rather than bicontinuous network at this composition. These aggregates subsequently coalesce with increasing $[C_{12}mim][Tf_2N]$ concentration, initially to form globular fragments of a non-polar network, and ultimately a continuous, non-polar sub-phase. This coalescence appears to be all but complete by 52 mol% $[C_{12}mim][Tf_2N]$ according to negative γ values in the SANS fitting and aggregate analyses from the MD simulations. The observed shift in position of the PNPP to higher q (and associated reduction in d-spacing) as the concentration of C12 chains increases can be linked to the length scale of the bilayer structures present in the liquids (i.e. the separation of the polar network by the alkyl chains of the non-polar sub-phase). Analysis of the bulk-phase MD trajectories suggests that there is no significant change in C12 alkyl chain interdigitation with increasing mole fraction of $[C_{12}mim][Tf_2N]$ (see ESI for details). Thus, this small change in length scale appears not to be related to the degree of interdigitation. Rather, there seems to be a general contraction in the non-polar network with increasing mole fraction of $[C_{12}mim][Tf_2N]$ that maybe caused by small rearrangements in the relative morphologies of the two sub-phases (e.g. loss of branched connectivity within the polar network or fewer "decorating" $[C_2mim]^+$ cations).

These observations can be compared to the behavior of pure $[C_n\text{mim}][Tf_2N]$ ILs with

increasing alkyl chain length. The PNPP appears and grows in intensity in a similar way in the

mixtures and pure ILs. In addition, SANS modelling and MD aggregate analysis of the mixtures and

pure ILs[120] suggests that larger aggregates of alkyl chains begin to appear around $[C_4\text{mim}][Tf_2N]$ and

$[C_2\text{mim}]_{0.76}[C_{12}\text{mim}]_{0.24}[Tf_2N]$, which have similar non-polar volume fractions, with percolation of the

non-polar network occurring by around $[C_6\text{mim}][Tf_2N]$ and by 52 mol% $[C_{12}\text{mim}][Tf_2N]$ in the

mixtures. SANS fitting and MD simulations suggest that percolation occurs at slightly different

compositions, both are based on models with some degree of error so this can be expected, but both

agree that percolation is complete at 52 mol% $[C_{12}\text{mim}][Tf_2N]$. This suggests that the formation of

non-polar aggregates and their subsequent coalescence to form a bicontinuous network of polar and

non-polar domains in these ILs is driven primarily by the relative volume fractions of the non-polar

and polar parts of the system. However, the length scales of the non-polar domains are different in the

mixtures and pure ILs, being dictated by the length of the longest alkyl chain. Thus, it is possible to

relate some of the features of $[C_2\text{mim}]_{1-x}[C_{12}\text{mim}]_x[Tf_2N]$ mixtures to pure ILs with which they are

'equivalent' in terms of non-polar volume fraction, but not all. The IL mixtures are structurally

distinct from the pure ILs.

This picture of the self-organized structure of the $[C_2\text{mim}]_{1-x}[C_{12}\text{mim}]_x[Tf_2N]$ mixtures can be

summarized visually in the four selected MD simulation snapshots presented in figure 15. The

percolation of the non-polar sub-phase for the two mixtures richer in $[C_{12}\text{mim}][Tf_2N]$ is obvious in

figures 14c and 14d. The large non-polar domains are dominated by interconnected C12 chains (grey

beads) 'decorated' at their periphery by a few C2 chains (light green beads). Some of the latter can still

be found in the midst of the polar network (red/blue mesh), separated from the non-polar sub-phase.
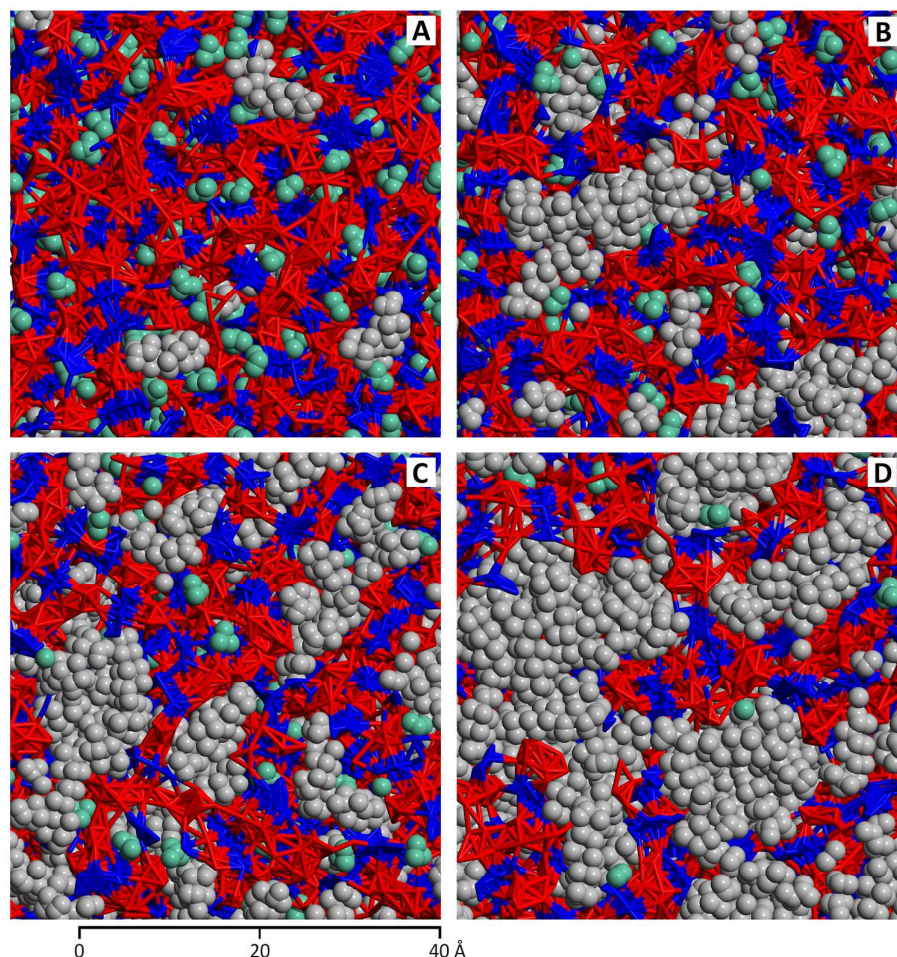
Figure 15: Four MD simulation snapshots illustrating the nano-segregation between the polar network (red/blue mesh) and non-polar domains (grey and green beads) in $[C_2mim]_{1-x}[C_{12}mim]_x[Tf_2N]$ (a) $x = 0.04$, (b) $x = 0.24$, (c) $x = 0.52$ and (d) $x = 0.87$. Atoms associated with the $[Tf_2N]^-$ ion are colored red. For $[C_2mim]^+$ and $[C_{12}mim]^+$ ions, the methyl substituent, imidazolium ring and the first methylene group of the alkyl substituent are shown in blue. All other atoms of the $[C_{12}mim]^+$ cation alkyl substituent are shown in grey.

Armed with this understanding of the bulk structure of the $[C_2mim]_{1-x}[C_{12}mim]_x[Tf_2N]$ mixtures, it is possible to propose why the physical properties of this system behave as they do with changing composition. In particular, the origins of the four key physical property observations that are highlighted above can be rationalized. Significant deviations from ideal behavior for the viscosities and conductivities of these mixtures become apparent at $x = 0.24$, with both sets of data suggesting

that ion mobility is lower than would be expected based on ideal mixing behavior. As discussed

above, this composition is composed mainly of small aggregates of C12 alkyl chains, but where larger

aggregates (up to around 60 chains, 17% of all C12 chains) can also be seen. It is proposed that it is

the presence of these larger aggregates, containing more connected C12 chains (which represent

fragments of a nascent non-polar network) that lead, through enhanced chain-chain interactions, to

lower ion mobility and the observed deviation from ideal behavior for the observed viscosities and

conductivities.

The fact that viscosity is the property that deviates most from ideal behavior in this system

could be linked to the reorganization of the longer-range ordering of the non-polar sub-phase that is

required in response to a shearing force. This may provide an additional resistance to flow alongside

local interionic interactions in the polar network. Recent work has suggested that network structures,

albeit based on rather different intermolecular interactions, formed in molten-salt mixtures also

contribute to higher than expected viscosities.[143-144] In these cases MD simulations using polarizable

force fields, which capture the dynamics of the systems more accurately, have shown that viscous

relaxation can be dominated by reorganization of network structures, which form as a function of their

composition, within the liquids. In the $[C_2mim]_{1-x}[C_{12}mim]_x[Tf_2N]$ mixtures, the fact that the

conductivity deviates less significantly from ideal behavior than viscosity presumably indicates that a

subtly different mechanism for ion mobility operates in the presence of an applied electric field.

The observation that density/excess molar volume data for the $[C_2mim]_{1-x}[C_{12}mim]_x[Tf_2N]$

mixtures deviate relatively little from ideal behavior compared with viscosity and conductivity data

suggests that overall, the sum of all interionic interactions changes relatively little when $[C_2mim]^+$

ions are substituted for $[C_{12}mim]^+$ ions. However, the small deviations from ideality that are observed

(lower densities and small, positive excess molar volumes) are consistent with slightly weakened

overall ion-ion interactions, consistent with the shift in COP position to lower q in SAXS experiments

(slightly longer cation···cation/anion···anion separations), which may result from the disruption of the

polar network by the formation of the non-polar sub-phase.

The corresponding changes taking place at the surface of the mixtures as the composition is varied are now considered. Contrary to previous reports based on ARXPS measurements,[90] significant surface enrichment of C12 alkyl chains was seen in RAS-LIF experiments and MD simulations. The corresponding key features of the surface properties are: i) the surface deviates substantially from stoichiometry in terms of excess C12 chains, from the lowest values of x; ii) the deviation from stoichiometry is at a maximum in the region of $x = 0.24$; iii) there is a region at very high x where the behavior returns to the stoichiometric line; iv) even in pure $[C_{12}mim][Tf_2N]$ (*i.e*. at $x = 1$), the surface is not fully saturated with C12 chains.

The picture that has emerged from the RAS-LIF measurements, supported by the MD simulations, can be summarized in figure 16, which shows approximately two unit cells from the MD simulations of each mixture slab, viewed from the side (camera perpendicular to surface normal). Neat $[C_2mim][Tf_2N]$ shows no ordering at the vacuum liquid-interface. Figure 16 provides visual confirmation of $[C_{12}mim]^+$ surface enrichment at all mixture mole fractions of $[C_{12}mim][Tf_2N]$. At very low mol% of $[C_{12}mim][Tf_2N]$, there is a preference for the dodecyl chain of surface active $[C_{12}mim]^+$ ions to lay perpendicular to the interface-normal. However, in mixtures containing larger amounts of $[C_{12}mim][Tf_2N]$ the C12 chains are observed to assume a disordered but somewhat more upright position.

The propensity for C12 chains to occupy the surface at low x is clearly an expression of their relative energetic preference for the surface over the bulk in a dilute mixture in $[C_2mim][Tf_2N]$ compared to the same competition between surface and bulk in pure $[C_{12}mim][Tf_2N]$. This can be understood by a simple analogy to an amphiphilic surfactant in a polar solvent (here $[C_2mim][Tf_2N]$) where the amphiphile (in this case the $[C_{12}mim]^+$ ion) will occupy the surface preferentially to avoid unfavorable hydrophobic interactions. Data from SANS and MD simulations show that by $x = 0.24$, the $[C_{12}mim]^+$ ions form aggregates in the bulk and there is evidence that some of these aggregates are quite large, which is interpreted as arising from a hydrophobic effect. As such, these aggregates provide an alternative location for $[C_{12}mim]^+$ ions as x increases. The combination of surface and bulk analysis then suggests that by $x = 0.24$ the two environments compete quite well as locations for $[C_{12}mim]^+$ ions, so that the degree of surface enrichment increases more slowly. However, a thorough

35

analysis would also have to take into account cooperative behavior between the dodecyl chains at the surface. Visual inspection of the simulations in figures 13 (in particular) and 16 shows that there clearly is such cooperative behavior in the surface occupation by C12 chains, which tend to aggregate even at low values of x. This clustering is still apparent at higher mole fractions, including in neat $[C_{12}mim][Tf_2N]$. As noted earlier, the surface of pure $[C_{12}mim][Tf_2N]$ does not appear entirely saturated with alkyl chains. Indeed, the relatively large size of the $[Tf_2N]^-$ anion and the proximity of cation and anion near the surface means that 'true' saturation will not be achieved – *i.e.* the situation as visualized in Figure 13 is as saturated as this system can become, because the cations cannot pack more closely together than this. In conventional surfactant chemistry, addition of surfactant to water leads to a rapid reduction in the surface tension as the surfactants assemble at the surface, with a sharp change in slope when the critical micelle concentration (cmc) is reached. However, careful analysis and consideration of these IL mixtures, for which the C12 component is much more modestly surface active than a typical surfactant in aqueous solution, shows that the surface only becomes saturated relatively slowly and continues to change with $[C_{12}mim][Tf_2N]$ mole fraction all the way to $x = 1$. A cmc is not evident in this system and it is clear that surface saturation *per se* does not drive aggregation. Given that formation of aggregates in the $[C_2mim]_{1-x}[C_{12}mim]_x[Tf_2N]$ mixtures is observed by $x = 0.24$, at which composition the surface is clearly not saturated, it is clear that there is little real analogy between this IL mixture system and conventional aqueous solutions of surfactants. If the system were to be considered as a $[C_{12}mim][Tf_2N]$ surfactant dissolved in $[C_2mim][Tf_2N]$, the data suggest that its surface activity is relatively weak and so it is clear that bulk aggregation in this system is not driven by the absence of available surface sites.

Finally, it is observed (figure 12) that there is an initial, near stoichiometric, reduction in C12 surface coverage with the addition of a small proportion of $[C_2mim][Tf_2N]$ to neat $[C_{12}mim][Tf_2N]$. This is consistent with a primarily entropic, colligative effect, where the C2 chains distribute statistically amongst highly aggregated C12 chains at both the surface and in the bulk.
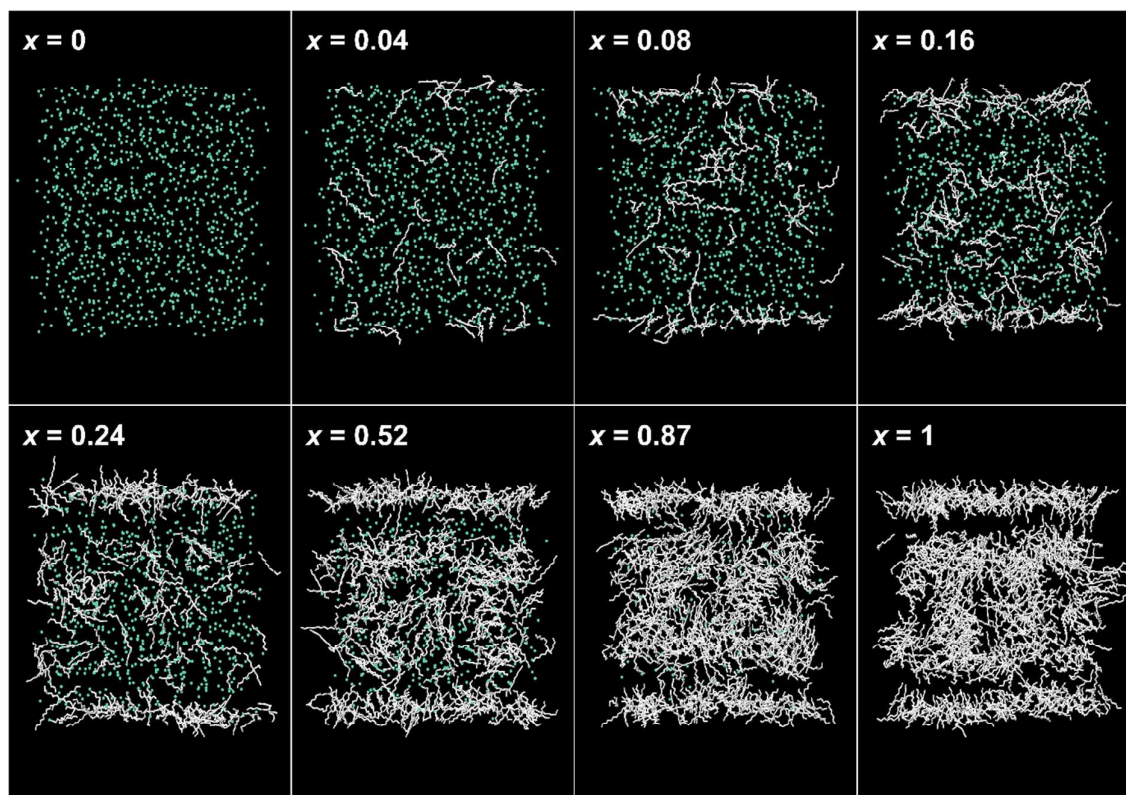
Figure 16: Side view of the vacuum-liquid surface of $[C_2mim]_{1-x}[C_{12}mim]_x[Tf_2N]$ mixtures. One unit cells is shown for each liquid. For clarity, only the non-polar parts of the cation alkyl groups are shown: $[C_2mim]^+$ methyl group on the ethyl chain is shown in green and $[C_{12}mim]^+$ final eleven carbon atoms of the dodecyl chain are shown in white.

Conclusions

In a comprehensive study, a range of approaches have been used to gain unprecedented insight into the bulk and surface structure of the binary IL mixtures $[C_2mim]_{1-x}[C_{12}mim]_x[Tf_2N]$ and have related this understanding to key physical properties of these liquids. Unlike some IL mixtures, the structure and properties of the $[C_2mim]_{1-x}[C_{12}mim]_x[Tf_2N]$ system are strongly dependent on composition. The IL surface structure is influenced substantially by composition, and, while previous studies have suggested otherwise,[90] clear evidence of surface enrichment of $[C_{12}mim]^+$ ions is found, with this effect being most pronounced around $x = 0.24$. At low mole fractions of $[C_{12}mim][Tf_2N]$, the bulk physical properties (viscosities and conductivities) show no significant deviation from ideal behavior. However, from $x = 0.24$ onwards these properties behave in a non-ideal way. At this composition,

larger aggregates of C12 alkyl chains are present in the liquid, which coalesce with increasing x to form a continuous non-polar sub-phase by $x = 0.52$ and it is proposed that increased chain-chain interactions in these larger aggregates are linked to the observed deviations in viscosities and conductivities. The length scales measured by scattering studies demonstrate that these IL mixtures are structurally distinct from pure ILs with which they share similar non-polar volume fractions. In the systems studied, the length scale of local bilayer structure in the liquids is clearly related to the length of the longest alkyl chain in the IL. However, the appearance of the PNPP in SAXS and SANS studies and the progression from small non-polar alkyl-chain aggregates to a continuous non-polar sub-phase in MD simulations do show some correlation with the non-polar volume fraction of both the pure ILs and mixtures. To sum up, there are some similarities and some differences between the IL mixtures investigated here and related pure ILs, but it is clear that they are a distinct system. The observations reported here are exciting, as they show that a range of structural and physical properties, both in the bulk and at the surface, can be controlled simply by the composition of an IL mixture, rather than by synthesizing a large number of pure ILs. The detailed understanding that this work brings promises to allow the rational selection of specific surface or bulk structure/properties in $[C_2mim]_{1-x}[C_{12}mim]_x[Tf_2N]$ mixtures when they are being considered for particular applications.

Supporting Information.

Full experimental and computational details are given in the supplementary information.

Schatz, Northwestern University, for helpful discussions and other input into the project. All data

created during this research are available by request from the University of York Data Catalogue.

References

1. Wasserscheid, P.; Welton, T., *Ionic Liquids in Synthesis*, 2nd ed.; Wiley-VCH: Weinheim, 2008.
2. Zhao, D. B.; Wu, M.; Kou, Y.; Min, E., Ionic Liquids: Applications in Catalysis. *Catal. Today* **2002**, *74*, 157-189.
3. Welton, T., Ionic Liquids in Catalysis. *Coord. Chem. Rev.* **2004**, *248*, 2459-2477.
4. Giernoth, R., Homogeneous Catalysis in Ionic Liquids. In *In Situ NMR Methods in Catalysis*, Bargon, J.; Kuhn, L. T., Eds. 2007; Vol. 276, pp 1-23.
5. Parvulescu, V. I.; Hardacre, C., Catalysis in Ionic Liquids. *Chem. Rev.* **2007**, *107*, 2615-2665.
6. Betz, D.; Altmann, P.; Cokoja, M.; Herrmann, W. A.; Kuehn, F. E., Recent Advances in Oxidation Catalysis Using Ionic Liquids as Solvents. *Coord. Chem. Rev.* **2011**, *255*, 1518-1540.
7. Zhang, Q.; Zhang, S.; Deng, Y., Recent Advances in Ionic Liquid Catalysis. *Green Chem.* **2011**, *13*, 2619-2637.
8. Welton, T., Room-Temperature Ionic Liquids. Solvents for Synthesis and Catalysis. *Chem. Rev.* **1999**, *99*, 2071-2083.
9. Sheldon, R. A.; Lau, R. M.; Sorgedrager, M. J.; van Rantwijk, F.; Seddon, K. R., Biocatalysis in Ionic Liquids. *Green Chem.* **2002**, *4*, 147-151.
10. Hallett, J. P.; Welton, T., Room-Temperature Ionic Liquids: Solvents for Synthesis and Catalysis. 2. *Chem. Rev.* **2011**, *111*, 3508-3576.
11. Endres, F.; MacFarlane, D.; Abbott, A., *Electrodeposition from Ionic Liquids*; Wiley-VCH: Weinheim, 2008.
12. Ohno, H., *Electrochemical Aspects of Ionic Liquids*; Wiley-Interscience: New Jersey, 2005.
13. Liu, F.; Deng, Y. D.; Han, X. P.; Hu, W. B.; Zhong, C., Electrodeposition of Metals and Alloys from Ionic Liquids. *J. Alloys Compd.* **2016**, *654*, 163-170.
14. Endres, F.; Bukowski, M.; Hempelmann, R.; Natter, H., Electrodeposition of Nanocrystalline Metals and Alloys from Ionic Liquids. *Angew. Chem., Int. Ed.* **2003**, *42*, 3428-3430.
15. Abbott, A. P.; McKenzie, K. J., Application of Ionic Liquids to the Electrodeposition of Metals. *Phys. Chem. Chem. Phys.* **2006**, *8*, 4265-4279.
16. Endres, F., Ionic Liquids: Solvents for the Electrodeposition of Metals and Semiconductors. *ChemPhysChem* **2002**, *3*, 144-154.
17. Dupont, J.; Scholten, J. D., On the Structural and Surface Properties of Transition-Metal Nanoparticles in Ionic Liquids. *Chem. Soc. Rev.* **2010**, *39*, 1780-1804.
18. Luska, K. L.; Migowski, P.; Leitner, W., Ionic Liquid-Stabilized Nanoparticles as Catalysts for the Conversion of Biomass. *Green Chem.* **2015**, *17*, 3195-3206.
19. Scholten, J. D.; Leal, B. C.; Dupont, J., Transition Metal Nanoparticle Catalysis in Ionic Liquids. *Acs Catal.* **2012**, *2*, 184-200.
20. Vollmer, C.; Janiak, C., Naked Metal Nanoparticles from Metal Carbonyls in Ionic Liquids: Easy Synthesis and Stabilization. *Coord. Chem. Rev.* **2011**, *255*, 2039-2057.
21. Prechtl, M. H. G.; Campbell, P. S., Metal Oxide and Bimetallic Nanoparticles in Ionic Liquids: Synthesis and Application in Multiphase Catalysis. *Nanotech. Rev.* **2013**, *2*, 577-595.
22. Antonietti, M.; Kuang, D. B.; Smarsly, B.; Yong, Z., Ionic Liquids for the Convenient Synthesis of Functional Nanoparticles and Other Inorganic Nanostructures. *Angew. Chem., Int. Ed.* **2004**, *43*, 4988-4992.
23. Torimoto, T.; Tsuda, T.; Okazaki, K.; Kuwabata, S., New Frontiers in Materials Science Opened by Ionic Liquids. *Adv. Mater.* **2010**, *22*, 1196-1221.
24. Brandt, A.; Grasvik, J.; Hallett, J. P.; Welton, T., Deconstruction of Lignocellulosic Biomass with Ionic Liquids. *Green Chem.* **2013**, *15*, 550-583.

25.   Wang, C. M.; Luo, X. Y.; Zhu, X.; Cui, G. K.; Jiang, D. E.; Deng, D. S.; Li, H. R.; Dai, S., The Strategies for Improving Carbon Dioxide Chemisorption by Functionalized Ionic Liquids. *RSC Adv.* **2013**, *3*, 15518-15527.

26.   Ramdin, M.; de Loos, T. W.; Vlugt, T. J. H., State-of-the-Art of CO_2 Capture with Ionic Liquids. *Ind. Eng. Chem. Res.* **2012**, *51*, 8149-8177.

27.   Anderson, J. L.; Armstrong, D. W.; Wei, G. T., Ionic Liquids in Analytical Chemistry. *Anal. Chem.* **2006**, *78*, 2892-2902.

28.   Pandey, S., Analytical Applications of Room-Temperature Ionic Liquids: A Review of Recent Efforts. *Anal. Chim. Acta* **2006**, *556*, 38-45.

29.   Han, X.; Armstrong, D. W., Ionic Liquids in Separations. *Acc. Chem. Res.* **2007**, *40*, 1079-1086.

30.   Berthod, A.; Ruiz-Angel, M.; Carda-Broch, S., Ionic Liquids in Separation Techniques. *J Chromatogr. A* **2008**, *1184*, 6-18.

31.   Sun, P.; Armstrong, D. W., Ionic Liquids in Analytical Chemistry. *Anal. Chim. Acta* **2010**, *661*, 1-16.

32.   Ho, T. D.; Zhang, C.; Hantao, L. W.; Anderson, J. L., Ionic Liquids in Analytical Chemistry: Fundamentals, Advances, and Perspectives. *Anal. Chem.* **2014**, *86*, 262-285.

33.   Niedermeyer, H.; Hallett, J. P.; Villar-Garcia, I. J.; Hunt, P. A.; Welton, T., Mixtures of Ionic Liquids. *Chem. Soc. Rev.* **2012**, *41*, 7780-7802.

34.   Chatel, G.; Pereira, J. F. B.; Debbeti, V.; Wang, H.; Rogers, R. D., Mixing Ionic Liquids - "Simple Mixtures" or "Double Salts"? *Green Chem.* **2014**, *16*, 2051-2083.

35.   Hayes, R.; Warr, G. G.; Atkin, R., Structure and Nanostructure in Ionic Liquids. *Chem. Rev.* **2015**, *115*, 6357-6426.

36.   Lovelock, K. R. J., Influence of the Ionic Liquid/Gas Surface on Ionic Liquid Chemistry. *Phys. Chem. Chem. Phys.* **2012**, *14*, 5071-5089.

37.   Lopes, J. N. A. C.; Padua, A. A. H., Nanostructural Organization in Ionic Liquids. *J. Phys. Chem. B* **2006**, *110*, 3330-3335.

38.   Egashira, M.; Okada, S.; Yamaki, J., The Effect of the Coexistence of Anion Species in Imidazolium Cation-Based Molten Salt Systems. *Solid State Ionics* **2002**, *148*, 457-461.

39.   Navia, P.; Troncoso, J.; Romani, L., Viscosities for Ionic Liquid Binary Mixtures with a Common Ion. *J. Solution Chem.* **2008**, *37*, 677-688.

40.   Stoppa, A.; Buchner, R.; Hefter, G., How Ideal Are Binary Mixtures of Room-Temperature Ionic Liquids? *J. Mol. Liq.* **2010**, *153*, 46-51.

41.   Annat, G.; Forsyth, M.; MacFarlane, D. R., Ionic Liquid Mixtures-Variations in Physical Properties and Their Origins in Molecular Structure. *J. Phys. Chem. B* **2012**, *116*, 8251-8258.

42.   Aparicio, S.; Atilhan, M., Mixed Ionic Liquids: The Case of Pyridinium-Based Fluids. *J. Phys. Chem. B* **2012**, *116*, 2526-2537.

43.   Kakibe, T.; Hishii, J. Y.; Yoshimoto, N.; Egashira, M.; Morita, M., Binary Ionic Liquid Electrolytes Containing Organo-Magnesium Complex for Rechargeable Magnesium Batteries. *J. Power Sources* **2012**, *203*, 195-200.

44.   Larriba, M.; Garcia, S.; Navarro, P.; Garcia, J.; Rodriguez, F., Physical Properties of N-Butylpyridinium Tetrafluoroborate and N-Butylpyridinium Bis(Trifluoromethylsulfonyl)Imide Binary Ionic Liquid Mixtures. *J. Chem. Eng. Data* **2012**, *57*, 1318-1325.

45.   Ning, H.; Hou, M. Q.; Mei, Q. Q.; Liu, Y. H.; Yang, D. Z.; Han, B. X., The Physicochemical Properties of Some Imidazolium-Based Ionic Liquids and Their Binary Mixtures. *Sci. China. Chem.* **2012**, *55*, 1509-1518.

46.   Song, D. Y.; Chen, J., Densities and Viscosities for Ionic Liquids Mixtures Containing Eohmim Bf4 , Bmim Bf4 and Bpy Bf4. *J. Chem. Thermodyn.* **2014**, *77*, 137-143.

47.   Song, D. Y.; Chen, J., Density and Viscosity Data for Mixtures of Ionic Liquids with a Common Anion. *J. Chem. Eng. Data* **2014**, *59*, 257-262.

48.   Larriba, M.; Navarro, P.; Beigbeder, J. B.; Garcia, J.; Rodriguez, F., Mixing and Decomposition Behavior of { 4bmpy Tf_2N + emim $EtSO_4$ } and { 4bmpy Tf_2N + emim TfES } Ionic Liquid Mixtures. *J. Chem. Thermodyn.* **2015**, *82*, 58-75.

49.   Stolarska, O.; Soto, A.; Rodriguez, H.; Smiglak, M., Properties Modification by Eutectic Formation in Mixtures of Ionic Liquids. *RSC Adv.* **2015**, *5*, 22178-22187.

50. Pinto, A. M.; Rodriguez, H.; Colon, Y. J.; Arce, A.; Arce, A.; Soto, A., Absorption of Carbon Dioxide in Two Binary Mixtures of Ionic Liquids. *Ind. Eng. Chem. Res.* **2013**, *52*, 5975-5984.

51. Fox, E. T.; Weaver, J. E. F.; Henderson, W. A., Tuning Binary Ionic Liquid Mixtures: Linking Alkyl Chain Length to Phase Behavior and Ionic Conductivity. *J. Phys. Chem. C.* **2012**, *116*, 5270-5274.

52. Castiglione, F.; Raos, G.; Battista Appetecchi, G.; Montanino, M.; Passerini, S.; Moreno, M.; Famulari, A.; Mele, A., Blending Ionic Liquids: How Physico-Chemical Properties Change. *Phys. Chem. Chem. Phys.* **2010**, *12*, 1784-1792.

53. Clough, M. T.; Crick, C. R.; Gräsvik, J.; Hunt, P. A.; Niedermeyer, H.; Welton, T.; Whitakerb, O. P., A Physicochemical Investigation of Ionic Liquid Mixtures. *Chem. Sci.* **2015**, *215*, 1101–1114.

54. Every, H.; Bishop, A. G.; Forsyth, M.; MacFarlane, D. R., Ion Diffusion in Molten Salt Mixtures. *Electrochim. Acta* **2000**, *45*, 1279-1284.

55. Bayley, P. M.; Best, A. S.; MacFarlane, D. R.; Forsyth, M., Transport Properties and Phase Behaviour in Binary and Ternary Ionic Liquid Electrolyte Systems of Interest in Lithium Batteries. *ChemPhysChem* **2011**, *12*, 823-827.

56. Taige, M. A.; Hilbert, D.; Schubert, T. J. S., Mixtures of Ionic Liquids as Possible Electrolytes for Lithium Ion Batteries. *Z. Phys. Chem.* **2012**, *226*, 129-139.

57. Lopes, J. N. C.; Cordeiro, T. C.; Esperanca, J. M. S. S.; Guedes, H. J. R.; Huq, S.; Rebelo, L. P. N.; Seddon, K. R., Deviations from Ideality in Mixtures of Two Ionic Liquids Containing a Common Ion. *J. Phys. Chem. B* **2005**, *109*, 3519-3525.

58. Navia, P.; Troncoso, J.; Romani, L., Excess Magnitudes for Ionic Liquid Binary Mixtures with a Common Ion. *J. Chem. Eng. Data* **2007**, *52*, 1369-1374.

59. Timperman, L.; Vigeant, A.; Anouti, M., Eutectic Mixture of Protic Ionic Liquids as an Electrolyte for Activated Carbon-Based Supercapacitors. *Electrochim. Acta* **2015**, *155*, 164-173.

60. Khupse, N. D.; Kurolikar, S. R.; Kumar, A., Temperature Dependent Viscosity of Mixtures of Ionic Liquids at Different Compositions. *Indian J Chem A* **2010**, *49*, 727-730.

61. Fumino, K.; Bonsa, A. M.; Golub, B.; Paschek, D.; Ludwig, R., Non-Ideal Mixing Behaviour of Hydrogen Bonding in Mixtures of Protic Ionic Liquids. *ChemPhysChem* **2015**, *16*, 299-304.

62. Maximo, G. J.; Santos, R.; Brandao, P.; Esperanca, J.; Costa, M. C.; Meirelles, A. J. A.; Freire, M. G.; Coutinho, J. A. P., Generating Ionic Liquids from Ionic Solids: An Investigation of the Melting Behavior of Binary Mixtures of Ionic Liquids. *Cryst. Growth Des.* **2014**, *14*, 4270-4277.

63. Shimizu, K.; Tariq, M.; Rebelo, L. P. N.; Lopes, J. N. C., Binary Mixtures of Ionic Liquids with a Common Ion Revisited: A Molecular Dynamics Simulation Study. *J. Mol. Liq.* **2010**, *153*, 52-56.

64. Llovell, F.; Valente, E.; Vilaseca, O.; Vega, L. F., Modeling Complex Associating Mixtures with C-N-Mim Tf$_2$N Ionic Liquids: Predictions from the Soft-Saft Equation. *J. Phys. Chem. B* **2011**, *115*, 4387-4398.

65. Brussel, M.; Brehm, M.; Pensado, A. S.; Malberg, F.; Ramzan, M.; Stark, A.; Kirchner, B., On the Ideality of Binary Mixtures of Ionic Liquids. *Phys. Chem. Chem. Phys.* **2012**, *14*, 13204-13215.

66. Omar, S.; Lemus, J.; Ruiz, E.; Ferro, V. R.; Ortega, J.; Palomar, J., Ionic Liquid Mixtures-an Analysis of Their Mutual Miscibility. *J. Phys. Chem. B* **2014**, *118*, 2442-2450.

67. Palchowdhury, S.; Bhargava, B. L., Segregation of Ions at the Interface: Molecular Dynamics Studies of the Bulk and Liquid-Vapor Interface Structure of Equimolar Binary Mixtures of Ionic Liquids. *Phys. Chem. Chem. Phys.* **2015**, *17*, 19919-19928.

68. Paschek, D.; Golub, B.; Ludwig, R., Hydrogen Bonding in a Mixture of Protic Ionic Liquids: A Molecular Dynamics Simulation Study. *Phys. Chem. Chem. Phys.* **2015**, *17*, 8431-8440.

69. Zahn, S.; Stark, A., Order in the Chaos: The Secret of the Large Negative Entropy of Dissolving 1-Alkyl-3-Methylimidazolium Chloride in Trihexyltetradecylphosphonium Chloride. *Phys. Chem. Chem. Phys.* **2015**, *17*, 4034-4037.

70. Thomaier, S.; Kunz, W., Aggregates in Mixtures of Ionic Liquids. *J. Mol. Liq.* **2007**, *130*, 104-107.

1
2
3
4
5
6
7
8
9
10
11
12
13
14
15
16
17
18
19
20
21
22
23
24
25
26
27
28
29
30
31
32
33
34
35
36
37
38
39
40
41
42
43
44
45
46
47
48
49
50
51
52
53
54
55
56
57
58
59
60

71.   Zhao, Y. R.; Chen, X.; Wang, X. D., Liquid Crystalline Phases Self-Organized from a Surfactant-Like Ionic Liquid C(16)MIMCl in Ethylammonium Nitrate. *J. Phys. Chem. B* **2009**, *113*, 2024-2030.

72.   Heintz, A.; Lehmann, J. K.; Kozlova, S. A.; Balantseva, E. V.; Bazyleva, A. B.; Ondo, D., Micelle Formation of Alkylimidazolium Ionic Liquids in Water and in Ethylammonium Nitrate Ionic Liquid: A Calorimetric Study. *Fluid Phase Equilib.* **2010**, *294*, 187-196.

73.   Kang, W. P.; Dong, B.; Gao, Y. N.; Zheng, L. Q., Aggregation Behavior of Long-Chain Imidazolium Ionic Liquids in Ethylammonium Nitrate. *Colloid Polym. Sci.* **2010**, *288*, 1225-1232.

74.   Shi, L.; Zhao, M.; Zheng, L., Micelle Formation by N-Alkyl-N-Methylpyrrolidinium Bromide in Ethylammonium Nitrate. *Colloids Surf. A* **2011**, *392*, 305-312.

75.   Shi, L. J.; Zheng, L. Q., Aggregation Behavior of Surface Active Imidazolium Ionic Liquids in Ethylammonium Nitrate: Effect of Alkyl Chain Length, Cations, and Counterions. *J. Phys. Chem. B* **2012**, *116*, 2162-2172.

76.   Dai, C.; Du, M. Y.; Liu, Y. F.; Wang, S. L.; Zhao, J. H.; Chen, A.; Peng, D. X.; Zhao, M. W., Aggregation Behavior of Long-Chain Piperidinium Ionic Liquids in Ethylammonium Nitrate. *Molecules* **2014**, *19*, 20157-20169.

77.   Li, N.; Zhang, S. H.; Zheng, L. Q.; Dong, B.; Li, X. W.; Yu, L., Aggregation Behavior of Long-Chain Ionic Liquids in an Ionic Liquid. *Phys. Chem. Chem. Phys.* **2008**, *10*, 4375-4377.

78.   Shi, L. J.; Li, N.; Zheng, L. Q., Aggregation Behavior of Long-Chain N-Aryl Lmidazolium Bromide in a Room Temperature Ionic Liquid. *J. Phys. Chem. C* **2011**, *115*, 18295-18301.

79.   Klee, A.; Prevost, S.; Gradzielski, M., Self-Assembly of Imidazolium-Based Surfactants in Magnetic Room-Temperature Ionic Liquids: Binary Mixtures. *ChemPhysChem* **2014**, *15*, 4032-4041.

80.   Greaves, T. L.; Drummond, C. J., Ionic Liquids as Amphiphile Self-Assembly Media. *Chem. Soc. Rev.* **2008**, *37*, 1709-1726.

81.   Greaves, T. L.; Drummond, C. J., Solvent Nanostructure, the Solvophobic Effect and Amphiphile Self-Assembly in Ionic Liquids. *Chem. Soc. Rev.* **2013**, *42*, 1096-1120.

82.   Villar-Garcia, I. J.; Fearn, S.; De Gregorio, G. F.; Ismail, N. L.; Gschwend, F. J. V.; McIntosh, A. J. S.; Lovelock, K. R. J., The Ionic Liquid-Vacuum Outer Atomic Surface: A Low-Energy Ion Scattering Study. *Chem. Sci.* **2014**, *5*, 4404-4418.

83.   Tesa-Serrate, M. A.; Marshall, B. C.; Smoll, E. J.; Purcell, S. M.; Costen, M. L.; Slattery, J. M.; Minton, T. K.; McKendrick, K. G., Ionic Liquid-Vacuum Interfaces Probed by Reactive Atom Scattering: Influence of Alkyl Chain Length and Anion Volume. *J. Phys. Chem. C* **2015**, *119*, 5491-5505.

84.   Villar-Garcia, I. J.; Fearn, S.; Ismail, N. L.; McIntosh, A. J. S.; Lovelock, K. R. J., Fine Tuning the Ionic Liquid-Vacuum Outer Atomic Surface Using Ion Mixtures. *Chem. Commun.* **2015**, *51*, 5367-5370.

85.   Ziemkiewich, M. P.; Zutz, A.; Nesbitt, D. J., Inelastic Scattering of Radicals at the Gas-Ionic Liquid Interface: Probing Surface Dynamics of BMIM-Cl, BMIM-BF$_4$, and BMIM-Tf$_2$N by Rovibronic Scattering of No [(2)Pi(1/2)(0.5)]. *J. Phys. Chem. C* **2012**, *116*, 14284-14294.

86.   Nakajima, K.; Miyashita, M.; Suzuki, M.; Kimura, K., Surface Structures of Binary Mixtures of Imidazolium-Based Ionic Liquids Using High-Resolution Rutherford Backscattering Spectroscopy and Time of Flight Secondary Ion Mass Spectroscopy. *J. Chem. Phys.* **2013**, *139*, 224701.

87.   Wu, B. H.; Zhang, J. M.; Minton, T. K.; McKendrick, K. G.; Slattery, J. M.; Yockel, S.; Schatz, G. C., Scattering Dynamics of Hyperthermal Oxygen Atoms on Ionic Liquid Surfaces: [EMIM][NTf$_2$] and [C$_{12}$MIM][NTf$_2$]. *J. Phys. Chem. C* **2010**, *114*, 4015-4027.

88.   Oliveira, M. B.; Dominguez-Perez, M.; Freire, M. G.; Llovell, F.; Cabeza, O.; Lopes-da-Silva, J. A.; Vega, L. F.; Coutinho, J. A. P., Surface Tension of Binary Mixtures of 1-Alkyl-3-Methylimidazolium Bis(trifluoromethylsulfonyl)imide Ionic Liquids: Experimental Measurements and Soft-Saft Modeling. *J. Phys. Chem. B* **2012**, *116*, 12133-12141.

89.   Oliveira, M. B.; Dominguez-Perez, M.; Cabeza, O.; Lopes-da-Silva, J. A.; Freire, M. G.; Coutinho, J. A. P., Surface Tensions of Binary Mixtures of Ionic Liquids with Bis(trifluoromethylsulfonyl)imide as the Common Anion. *J. Chem. Thermodyn.* **2013**, *64*, 22-27.

90.   Maier, F.; Cremer, T.; Kolbeck, C.; Lovelock, K. R. J.; Paape, N.; Schulz, P. S.; Wasserscheidc, P.; Steinruck, H. P., Insights into the Surface Composition and Enrichment Effects of Ionic Liquids and Ionic Liquid Mixtures. *Phys. Chem. Chem. Phys.* **2010**, *12*, 1905-1915.

91.   Nakajima, K.; Oshima, S.; Suzuki, M.; Kimura, K., Surface Structures of Equimolar Mixtures of Imidazolium-Based Ionic Liquids Using High-Resolution Rutherford Backscattering Spectroscopy. *Surf. Sci.* **2012**, *606*, 1693-1699.

92.   Souda, R., Surface Segregation in Binary Mixtures of Imidazolium-Based Ionic Liquids. *Surf. Sci.* **2010**, *604*, 1694-1697.

93.   Waring, C.; Bagot, P. A. J.; Slattery, J. M.; Costen, M. L.; McKendrick, K. G., O(3P) Atoms as a Chemical Probe of Surface Ordering in Ionic Liquids. *J. Phys. Chem. A* **2010**, *114*, 4896-4904.

94.   Waring, C.; Bagot, P. A. J.; Slattery, J. M.; Costen, M. L.; McKendrick, K. G., O(3P) Atoms as a Probe of Surface Ordering in 1-Alkyl-3-Methylimidazolium-Based Ionic Liquids. *J. Phys. Chem. Lett.* **2010**, *1*, 429-433.

95.   Bhargava, B. L.; Balasubramanian, S., Layering at an Ionic Liquid-Vapor Interface: A Molecular Dynamics Simulation Study of [BMIM][PF$_6$]. *J. Am. Chem. Soc.* **2006**, *128*, 10073-10078.

96.   Garcia, G.; Atilhan, M.; Aparicio, S., Interfacial Properties of Double Salt Ionic Liquids: A Molecular Dynamics Study. *J. Phys. Chem. C* **2015**, *119*, 28405-28416.

97.   Shimizu, K.; Lopes, J. N. C., Probing the Structural Features of the 1-Alkyl-3-Methylimidazolium Hexafluorophosphate Ionic Liquid Series Using Molecular Dynamics Simulations. *J. Mol. Liq.* **2015**, *210*, 257-263.

98.   Arrhenius, S., Origin of Grunberg-Nissan Mixing Law. *Z. Phys. Chem.* **1887**, *1*, 285.

99.   Powell, R. E.; Roseveare, W. E.; Eyring, H., Diffusion, Thermal Conductivity, and Viscous Flow of Liquids. *Ind. Eng. Chem.* **1941**, *33*, 430-435.

100.   Grunberg, L.; Nissan, A. H., Mixture Law for Viscosity. *Nature* **1949**, *164*, 799-800.

101.   Katti, P. K.; Chaudhri, M. M., Viscosities of Binary Mixtures of Benzyl Acetate with Dioxane, Aniline, and M-Cresol. *J. Chem. Eng. Data* **1964**, *9*, 442-443.

102.   MacFarlane, D. R.; Forsyth, M.; Izgorodina, E. I.; Abbott, A. P.; Annat, G.; Fraser, K., On the Concept of Ionicity in Ionic Liquids. *Phys. Chem. Chem. Phys.* **2009**, *11*, 4962-4967.

103.   Pinkert, A.; Ang, K. L.; Marsh, K. N.; Pang, S. S., Density, Viscosity and Electrical Conductivity of Protic Alkanolammonium Ionic Liquids. *Phys. Chem. Chem. Phys.* **2011**, *13*, 5136-5143.

104.   Schreiner, C.; Zugmann, S.; Hartl, R.; Gores, H. J., Fractional Walden Rule for Ionic Liquids: Examples from Recent Measurements and a Critique of the So-Called Ideal Kcl Line for the Walden Plot. *J. Chem. Eng. Data* **2010**, *55*, 1784-1788.

105.   Annapureddy, H. V. R.; Kashyap, H. K.; De Biase, P. M.; Margulis, C. J., What Is the Origin of the Prepeak in the X-Ray Scattering of Imidazolium-Based Room-Temperature Ionic Liquids? *J. Phys. Chem. B* **2010**, *114*, 16838-16846.

106.   Gontrani, L.; Russina, O.; Lo Celso, F.; Caminiti, R.; Annat, G.; Triolo, A., Liquid Structure of Trihexyltetradecylphosphonium Chloride at Ambient Temperature: An X-Ray Scattering and Simulation Study. *J. Phys. Chem. B* **2009**, *113*, 9235-9240.

107.   Hettige, J. J.; Kashyap, H. K.; Annapureddy, H. V. R.; Margulis, C. J., Anions, the Reporters of Structure in Ionic Liquids. *J. Phys. Chem. Lett.* **2013**, *4*, 105-110.

108.   Kashyap, H. K.; Hettige, J. J.; Annapureddy, H. V. R.; Margulis, C. J., Saxs Anti-Peaks Reveal the Length-Scales of Dual Positive-Negative and Polar-Apolar Ordering in Room-Temperature Ionic Liquids. *Chem. Commun.* **2012**, *48*, 5103-5105.

109.   Rocha, M. A. A.; Neves, C. M. S. S.; Freire, M. G.; Russina, O.; Triolo, A.; Coutinho, J. A. P.; Santos, L. M. N. B. F., Alkylimidazolium Based Ionic Liquids: Impact of Cation Symmetry on Their Nanoscale Structural Organization. *J. Phys. Chem. B* **2013**, *117*, 10889-10897.

110.   Russina, O.; Gontrani, L.; Fazio, B.; Lombardo, D.; Triolo, A.; Caminiti, R., Selected Chemical-Physical Properties and Structural Heterogeneities in 1-Ethyl-3-Methylimidazolium Alkyl-Sulfate Room Temperature Ionic Liquids. *Chem. Phys. Lett.* **2010**, *493*, 259-262.

111.   Russina, O.; Triolo, A., New Experimental Evidence Supporting the Mesoscopic Segregation Model in Room Temperature Ionic Liquids. *Faraday Discuss.* **2012**, *154*, 97-109.

112.   Russina, O.; Triolo, A.; Gontrani, L.; Caminiti, R., Mesoscopic Structural Heterogeneities in Room-Temperature Ionic Liquids. *J. Phys. Chem. Lett.* **2012**, *3*, 27-33.

113.   Russina, O.; Triolo, A.; Gontrani, L.; Caminiti, R.; Xiao, D.; Hines, L. G.; Bartsch, R. A.; Quitevis, E. L.; Plechkova, N.; Seddon, K. R., Morphology and Intermolecular Dynamics of 1-Alkyl-

3-Methylimidazolium Bis{(Trifluoromethane)Sulfonyl}Amide Ionic Liquids: Structural and Dynamic Evidence of Nanoscale Segregation. *J. Phys.: Condens. Mat.* **2009**, *21*.

114. Triolo, A.; Russina, O.; Bleif, H. J.; Di Cola, E., Nanoscale Segregation in Room Temperature Ionic Liquids. *J. Phys. Chem. B* **2007**, *111*, 4641-4644.

115. Triolo, A.; Russina, O.; Caminiti, R.; Shirota, H.; Lee, H. Y.; Santos, C. S.; Murthy, N. S.; Castner, E. W., Comparing Intermediate Range Order for Alkyl- Vs. Ether-Substituted Cations in Ionic Liquids. *Chem. Commun.* **2012**, *48*, 4959-4961.

116. Triolo, A.; Russina, O.; Fazio, B.; Appetecchi, G. B.; Carewska, M.; Passerini, S., Nanoscale Organization in Piperidinium-Based Room Temperature Ionic Liquids. *J. Chem. Phys.* **2009**, *130*.

117. Triolo, A.; Russina, O.; Fazio, B.; Triolo, R.; Di Cola, E., Morphology of 1-Alkyl-3-Methylimidazolium Hexafluorophosphate Room Temperature Ionic Liquids. *Chem. Phys. Lett.* **2008**, *457*, 362-365.

118. Xiao, D.; Hines, L. G.; Li, S. F.; Bartsch, R. A.; Quitevis, E. L.; Russina, O.; Triolo, A., Effect of Cation Symmetry and Alkyl Chain Length on the Structure and Intermolecular Dynamics of 1,3-Dialkylimidazolium Bis(Trifluoromethanesulfonyl)Amide Ionic Liquids. *J. Phys. Chem. B* **2009**, *113*, 6426-6433.

119. Zheng, W.; Mohammed, A.; Hines, L. G.; Xiao, D.; Martinez, O. J.; Bartsch, R. A.; Simon, S. L.; Russina, O.; Triolo, A.; Quitevis, E. L., Effect of Cation Symmetry on the Morphology and Physicochemical Properties of Imidazolium Ionic Liquids. *J. Phys. Chem. B* **2011**, *115*, 6572-6584.

120. Shimizu, K.; Bernardes, C. E. S.; Lopes, J. N. C., Structure and Aggregation in the 1-Alkyl-3-Methylimidazolium Bis(Trifluoromethylsulfonyl)Imide Ionic Liquid Homologous Series. *J. Phys. Chem. B* **2014**, *118*, 567-576.

121. Bernardes, C. E. S.; Shimizu, K.; Ferreira, A. I. M. C. L.; Santos, L. M. N. B. F.; Lopes, J. N. C., Structure and Aggregation in the 1,3-Dialkyl-Imidazolium Bis(Trifluoromethylsulfonyl)Imide Ionic Liquid Family: 2. From Single to Double Long Alkyl Side Chains. *J. Phys. Chem. B* **2014**, *118*, 6885-6895.

122. Schubert, K. V.; Strey, R.; Kline, S. R.; Kaler, E. W., Small-Angle Neutron-Scattering near Lifshitz Lines - Transition from Weakly Structured Mixtures to Microemulsions. *J. Chem. Phys.* **1994**, *101*, 5343-5355.

123. Teubner, M.; Strey, R., Origin of the Scattering Peak in Microemulsions. *J. Chem. Phys.* **1987**, *87*, 3195-3200.

124. Krossing, I.; Slattery, J. M.; Daguenet, C.; Dyson, P. J.; Oleinikova, A.; Weingartner, H., Why Are Ionic Liquids Liquid? A Simple Explanation Based on Lattice and Solvation Energies. *J. Am. Chem. Soc.* **2006**, *128*, 13427-13434.

125. Slattery, J. M.; Daguenet, C.; Dyson, P. J.; Schubert, T. J. S.; Krossing, I., How to Predict the Physical Properties of Ionic Liquids: A Volume-Based Approach. *Angew. Chem. Int. Ed.* **2007**, *46*, 5384-5388.

126. Bulut, S.; Eiden, P.; Beichel, W.; Slattery, J. M.; Beyersdorff, T. F.; Schubert, T. J. S.; Krossing, I., Temperature Dependence of the Viscosity and Conductivity of Mildly Functionalized and Non-Functionalized [Tf$_2$N]$^-$ Ionic Liquids. *ChemPhysChem* **2011**, *12*, 2296-2310.

127. Smith, W.; Forester, T. R. *The Dl_Poly Package of Molecular Simulation Routines (V.2.2)*, The Council for The Central Laboratory of Research Councils.: Warrington: Daresbury Laboratory, 2006.

128. Lopes, J. N. C.; Deschamps, J.; Padua, A. A. H., Modeling Ionic Liquids Using a Systematic All-Atom Force Field. *J. Phys. Chem. B* **2004**, *108*, 2038-2047.

129. Lopes, J. N. C.; Padua, A. A. H., Molecular Force Field for Ionic Liquids Composed of Triflate or Bistriflylimide Anions. *J. Phys. Chem. B* **2004**, *108*, 16893-16898.

130. Jorgensen, W. L.; Maxwell, D. S.; TiradoRives, J., Development and Testing of the Opls All-Atom Force Field on Conformational Energetics and Properties of Organic Liquids. *J. Am. Chem. Soc.* **1996**, *118*, 11225-11236.

131. Rebelo, L. P. N.; Lopes, J. N. C.; Esperanca, J. M. S. S.; Guedes, H. J. R.; Lachwa, J.; Najdanovic-Visak, V.; Visak, Z. P., Accounting for the Unique, Doubly Dual Nature of Ionic Liquids from a Molecular Thermodynamic, and Modeling Standpoint. *Accounts of Chemical Research* **2007**, *40*, 1114-1121.

44

132.   Freitas, A. A.; Shimizu, K.; Lopes, J. N. C., Complex Structure of Ionic Liquids. Molecular Dynamics Studies with Different Cation-Anion Combinations. *J. Chem. Eng. Data* **2014**, *59*, 3120-3129.

133.   Shimizu, K.; Tariq, M.; Freitas, A. A.; Padua, A. A. H.; Lopes, J. N. C., Self-Organization in Ionic Liquids: From Bulk to Interfaces and Films. *J. Braz. Chem. Soc.* **2016**, *27*, 349-362.

134.   Shimizu, K.; Lopes, J. N. C., Comparing the Structure of Different Ionic Liquid Series: Bistriflamide V. Hexafluorophosphate; Pure V. Equimolar Mixtures. *Fluid Phase Equilib.* **2016**, *418*, 181-191.

135.   Purcell, S. M.; Tesa-Serrate, M. A.; Marshall, B. C.; Bruce, D. W.; D'Andrea, L.; Costen, M. L.; Slattery, J. M.; Smoll, E. J.; Minton, T. K.; McKendrick, K. G., Reactive-Atom Scattering from Liquid Crystals at the Liquid-Vacuum Interface: [C$_{12}$MIM][BF$_4$] and 4-Cyano-4 '-Octylbiphenyl (8cb). *Langmuir* **2016**, *32*, 9938-9949.

136.   Tesa-Serrate, M. A.; Smoll, E. J.; D'Andrea, L.; Purcell, S. M.; Costen, M. L.; Bruce, D. W.; Slattery, J. M.; Minton, T. K.; McKendrick, K. G., Hiding the Headgroup? Remarkable Similarity in Alkyl Coverage of the Surfaces of Pyrrolidinium- and Imidazolium-Based Ionic Liquids. *J. Phys. Chem. C.* **2016**, *120*, 27369-27379.

137.   Tesa-Serrate, M. A.; Smoll, E. J.; Minton, T. K.; McKendrick, K. G., Atomic and Molecular Collisions at Liquid Surfaces. *Annual Review of Physical Chemistry, Vol 67* **2016**, *67*, 515-540.

138.   Lopes, J. N. A. C.; Padua, A. A. H.; Deschamps, J., Modeling Ionic Liquids Using an Extended Opls-Aa Force Field. *Abstr. Pap. Am. Chem. Soc.* **2003**, *226*, U618-U618.

139.   Lopes, J. N. C.; Deschamps, J.; Padua, A. A. H., Modeling Ionic Liquids Using a Systematic All-Atom Force Field. *J. Phys. Chem. B.* **2004**, *108*, 2038-2047.

140.   Lopes, J. N. C.; Padua, A. A. H., Molecular Force Field for Ionic Liquids Iii: Imidazolium, Pyridinium, and Phosphonium Cations; Chloride, Bromide, and Dicyanamide Anions. *J. Phys. Chem. B* **2006**, *110*, 19586-19592.

141.   Lopes, J. N. C.; Padua, A. A. H.; Shimizu, K., Molecular Force Field for Ionic Liquids Iv: Trialkylimidazolium and Alkoxycarbonyl-Imidazolium Cations; Alkylsulfonate and Alkylsulfate Anions. *J. Phys. Chem. B* **2008**, *112*, 5039-5046.

142.   Shimizu, K.; Almantariotis, D.; Gomes, M. F. C.; Padua, A. A. H.; Lopes, J. N. C., Molecular Force Field for Ionic Liquids V: Hydroxyethylimidazolium, Dimethoxy-2-Methylimidazolium, and Fluoroalkylimidazolium Cations and Bis(Fluorosulfonyl)Amide, Perfluoroalkanesulfonylamide, and Fluoroalkylfluorophosphate Anions. *J. Phys. Chem. B* **2010**, *114*, 3592-3600.

143.   Salanne, M.; Simon, C.; Turq, P.; Madden, P. A., Conductivity-Viscosity-Structure: Unpicking the Relationship in an Ionic Liquid. *J. Phys. Chem. B* **2007**, *111*, 4678-4684.

144.   Corradini, D.; Madden, P. A.; Salanne, M., Coordination Numbers and Physical Properties in Molten Salts and Their Mixtures. *Faraday Discuss.* **2016**, *190*, 471-486.

TOC Graphic